

Non-equilibrium time evolution and rephasing in the quantum sine-Gordon model

D. X. Horváth^{1,3}, I. Lovas^{2,3}, M. Kormos^{1,3}, G. Takács^{1,3} and G. Zaránd^{2,3}

¹BME "Momentum" Statistical Field Theory Research Group

1111 Budapest, Budafoki út 8, Hungary

²BME "Momentum" Exotic Quantum Phases Research Group

1111 Budapest, Budafoki út 8, Hungary

³Department of Theoretical Physics,

Budapest University of Technology and Economics

1111 Budapest, Budafoki út 8, Hungary

17th September 2018

Abstract

We discuss the non-equilibrium time evolution of the phase field in the sine-Gordon model using two very different approaches: the truncated Wigner approximation and the truncated conformal space approach. We demonstrate that the two approaches agree for a period covering the first few oscillations, thereby giving a solid theoretical prediction in the framework of sine-Gordon model, which is thought to describe the dynamics of two bosonic condensates in quasi-one-dimensional traps coupled via a Josephson tunneling term. We conclude, however, that the recently observed phase-locking behavior cannot be explained in terms of homogeneous sine-Gordon dynamics, which hints at the role of other degrees of freedom or inhomogeneity in the experimental system.

1 Introduction

In recent years, understanding the out-of-equilibrium phenomena of isolated quantum many-body systems has become a major challenge. The recent experimental realization of such systems spurred considerable interest and progress in the experimental and theoretical study of non-equilibrium behavior. In particular, the use of cold atomic gases led to controlled realizations of isolated quantum systems, and allowed the observation of a number of astonishing non-equilibrium phenomena [1, 2, 3, 4, 5, 6, 7, 8, 9]. These include the lack of thermalization in quantum integrable systems [1, 2, 3, 10] or the experimental confirmation [4] of the generalized Gibbs ensemble (GGE) [11] as the valid description of non-equilibrium steady states.

A particularly interesting experimental setup is provided by a bosonic Josephson junction, consisting of two coupled superfluids in parallel elongated traps [12, 13]. When the dynamics of the condensates is dominated by continuum 1D physics, the relative phase of the condensates can be described by the sine-Gordon model [14]. In thermal equilibrium and under suitable conditions, this fact was demonstrated experimentally in Ref. [15] by comparing the measured correlations to the prediction of classical thermal sine-Gordon model [16]. On the other hand, the out-of-equilibrium behavior of the system of the coupled condensates was found to display intriguing behavior such as a rapid phase-locking [17], so far unexplained from the dynamics of the sine-Gordon field theory.

In this work, we analyze this rephasing phenomenon within the theoretical framework of the homogeneous sine-Gordon model through a combination of two powerful though approximate methods: the Truncated Wigner Approximation (TWA) and the Truncated Conformal Space Approach (TCSA). We compare these two approaches in the strongly interacting regime, where we find an excellent agreement between them. However, our TWA results in the weakly interacting regime, relevant for the experiments, clearly disagree with experimental observations, thereby leading us to the conclusion that the homogeneous sine-Gordon model is *insufficient* to account for the experimental observations.

The sine-Gordon model has attracted interest since long [18, 19, 20], and is considered to be a paradigmatic example of an integrable quantum field theory [21, 22, 23]. Due to integrability, many quantities can be computed exactly, such as the scattering amplitudes [23], exact expectation values [24], and form factors [25]. Integrability allows the application of powerful methods to compute the long-distance expansion of zero-temperature two-point correlators [26], although only very limited results are available on quantum correlation functions under more general conditions, and they are mostly confined to one-point functions in thermal equilibrium [27, 28].

Therefore numerical and approximate methods are of great value and must also be invoked to understand these non-equilibrium systems. One possibility is to resort to a semiclassical description, which allows the construction of one- and two-point functions using a quasi-particle picture [29, 30]. Semiclassical methods can, however, only partially account for the quantum dynamics.

Here we apply an alternative approach, the so-called truncated Wigner approximation (TWA) [31, 32, 33], giving a slightly different quasi-classical approximation of the phase dynamics. Unfortunately, it is very hard to control the accuracy of TWA. TWA has so far only been validated by perturbation theory (that captures only the first peak in the evolution) and by a scaling law that simply follows from conformal field theory considerations. TWA predicts an interesting oscillation with slowly decaying amplitude at longer times [31]. However, as shown here, quantum corrections become dominant in this long time regime, and the TWA approximation becomes uncontrolled.

To validate the truncated Wigner approach at these longer times, we resort to the truncated conformal space approach (TCSA). This approach was originally introduced by Yurov and Zamolodchikov to describe the finite volume spectrum of two-dimensional QFTs [34], and it can be also used to describe non-equilibrium time evolution in quantum field theories [35], initial state overlaps [36] and multi-point correlation functions in and out of equilibrium [37].

Here we use the TCSA and the TWA approaches to examine phase locking during the first few oscillations with two initial conditions. The first corresponds to preparing two identical condensates independently in their ground state, and switching on tunneling at time zero. The other initial condition differs by preparing the two condensates with a well-defined difference of the atom numbers in the respective trap. For technical reasons, here we focus on homogeneous 1D systems with periodic boundary condition and neglect density inhomogeneities. Both initial conditions yield weakly damped oscillations even in the strongly interacting regime. The excellent agreement between TCSA and TWA provides a strong validation of the results presented here.

Before considering the sine-Gordon model in its full glory, we can gain a rough understanding of the dynamics by considering a single mode model of the condensates, corresponding to the quantum pendulum

$$H_{\text{pendulum}} = Un_0^2 - JN \cos \varphi_0, \quad (1)$$

where the canonical conjugate variables φ_0 and n_0 satisfy $[\varphi_0, n_0] = i$. Hamiltonian (1) describes the time evolution of the relative phase φ_0 and particle number difference n_0 . Here U characterizes the interaction between the atoms in the same condensate, J denotes the tunnel coupling between the potential wells, N is the total number of atoms, and Eq. (1) is valid in the regime of small

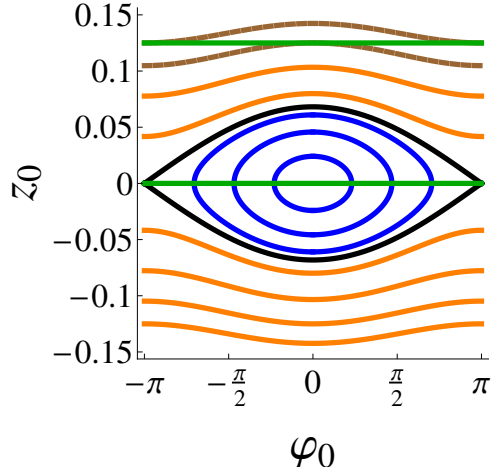


Figure 1: Classical trajectories of the pendulum model (1), plotted in terms of phase φ_0 and rescaled particle number difference $z_0 = 2n_0/N$. The separatrix (black) separates the self-trapped regime with trajectories constrained to $z_0 > 0$ or $z_0 < 0$ half-plane (orange), from the trajectories visiting both half-planes (blue). The initial states considered in Sec. 5, corresponding to a well-defined particle number difference and a random phase, can be visualised as horizontal lines (green, dashed). In the self-trapped regime, the small frequency shift between the trajectories cut by this line (brown) amounts to beating phenomena.

particle number difference $n_0 \ll N$.

Although for the quasi one dimensional condensates considered in this paper, fluctuations – incorporated in the sine-Gordon model – play an essential role, and the single mode approximation Eq. (1) breaks down, the dynamics of the pendulum model (1), nevertheless, still offers a qualitative understanding of the time evolution under the sine-Gordon Hamiltonian. We display the classical trajectories of the pendulum (1) in Fig. 1, determined by energy conservation

$$\frac{UN^2}{4}z_0^2 - JN \cos \varphi_0 = E, \quad (2)$$

with $z_0 = 2n_0/N$. For large enough E , the trajectories are confined to a self-trapped domain, constrained to the half-plane $z_0 > 0$ or $z_0 < 0$, since the high interaction energy prevents leveling off the number of particles in the two potential wells. This region is separated from the low energy trajectories, visiting both half planes, by a separatrix.

Both initial states considered in this work correspond to a well defined particle number difference n_0 , and to a uniformly distributed random phase φ_0 ; they are visualized as dashed horizontal lines in Fig. 1. The non-equilibrium dynamics can be qualitatively understood in terms of the classical trajectories intersected by these horizontal lines. To test TWA and TCSEA in both phases, first we consider two identical condensates in Sec. 5.1, corresponding to $n_0 = 0$, where the dynamics is determined by the classical trajectories lying in the non-trapped phase. Then in Sec. 5.2 we choose a large particle number imbalance n_0 , such that all relevant trajectories are self-trapped. Unfortunately, as we discuss below, for technical reasons we cannot compare the TCSEA and TWA methods for initial states intersecting the separatrix. Nevertheless, for initial states far enough from the boundary of self-trapping, we find an excellent agreement between TWA and TCSEA methods in both phases. Moreover, in the self-trapped phase all intersected trajectories lie in a narrow frequency window. As we discuss in Sec. 5.2, the non-equilibrium expectation values considered here oscillate

with the typical frequency of these classical trajectories, while the small frequency shift between the relevant trajectories gives rise to beating effects.

The outline of the paper is as follows. Sec. 2 reviews the necessary ingredients of the sine-Gordon description of the coupled quasi-1D condensates. In Sec. 3 we provide the detailed connections between the lattice regularized description used in the TWA and the perturbed conformal field theory framework of the TCSA, which allows for their detailed numerical comparison. Sec. 4 outlines the description of both the TWA and TCSA methods themselves, while the results for the two initial conditions are presented in Secs. 5.1 and 5.2, respectively. Finally, our conclusions are presented in Sec. 6. Certain technicalities are relegated to appendices: App. A provides more details on the mapping of the coupled condensates to a sine-Gordon model, App. B contains the technical details on normal ordering needed to compare observables between TWA and TCSA, App. C describes the extrapolation procedure used in TCSA to eliminate the leading truncation effects, while App. D reviews the derivation of the TWA and its leading quantum correction.

2 Sine-Gordon description of ultracold one-dimensional bosons

The physics of two Josephson-coupled one-dimensional interacting quasi-condensates can be described to a very good approximation by the sine-Gordon model. For a precise mapping, one usually considers two quasi one-dimensional gases, described by the Hamiltonians [38, 39]

$$H_0 = \sum_{j=1,2} \int dx \left\{ \frac{\hbar^2}{2m} \partial_x \psi_j^\dagger(x) \partial_x \psi_j(x) + \frac{g}{2} \psi_j^\dagger(x) \psi_j^\dagger(x) \psi_j(x) \psi_j(x) + [V(x) - \mu] \psi_j^\dagger(x) \psi_j(x) \right\}, \quad (3)$$

coupled by the Josephson tunneling term,

$$H_J = -J \int dx \left[\psi_1^\dagger(x) \psi_2(x) + \psi_2^\dagger(x) \psi_1(x) \right]. \quad (4)$$

Here $\psi_1(x), \psi_2(x)$ denote the bosonic fields of the two quasi-condensates, $V(x)$ is the longitudinal trap potential, J the tunneling amplitude, and g stands for the effective one-dimensional interaction [40]. In the rest of this paper, we shall neglect the trapping potential and focus on homogeneous condensates. Furthermore, since boundary conditions do not influence the dynamics discussed in an essential way, we shall impose periodic boundary conditions for the sake of simplicity.

The value of the coupling g depends sensitively on the shape of the transverse trapping potential, and can be approximated as [41]

$$g \approx \frac{2\hbar^2 a_s}{m l_\perp^2} \left(1 - 1.036 \frac{a_s}{l_\perp} \right)^{-1}, \quad (5)$$

with $l_\perp = \sqrt{\hbar/(m\omega_\perp)}$ the transverse oscillator length associated with the frequency ω_\perp of the radial confining potential, and a_s the three-dimensional s -wave scattering length of the atoms. For weak interactions, $a_s \ll l_\perp$, one simply obtains $g \approx 2\hbar\omega_\perp a_s$.

To describe this interacting system, one often refers to "bosonisation" [42], and represents the trapped bosons in terms of their phase φ_j and density ρ_j as

$$\psi_j(x) = \sqrt{\rho_j(x)} e^{i\varphi_j(x)}, \quad (6)$$

with the density fluctuations $\delta\rho_j(x)$ and the phase $\varphi_j(x)$ playing the role of conjugate variables. Substituting (6) into Eq. (3), one obtains a hydrodynamical description of the condensates. To

leading order in the density and phase fluctuations, the relative phase $\varphi_r = \varphi_2 - \varphi_1$ decouples from the total phase, $\varphi_1 + \varphi_2$ and the dynamics of the former is described by the sine-Gordon Hamiltonian,

$$H_r = \frac{\hbar c}{2} \int dx \left\{ \frac{\pi}{K} \Pi_r^2 + \frac{K}{\pi} (\partial_x \varphi_r)^2 \right\} - 2J\rho_0 \int dx \cos \varphi_r, \quad (7)$$

with Π_r the relative canonical momentum, c the sound velocity and K the so-called Luttinger parameter. For the homogeneous gas considered here the average density ρ_0 is related to the total number of atoms N confined the length L of the system as $\rho_0 = N/2L$. We note that K is a rather non-trivial function of the dimensionless interaction, $\gamma = mg/(\hbar^2 \rho_0)$ (see Appendix A); for weakly interacting bosons $K \gg 1$, while very strong atom-atom interactions yield $K \approx 1/2$.

The usual, field theoretical form of the sine-Gordon model can be obtained by setting $\hbar = c = 1$ and rescaling the relative field and momentum as $\sqrt{\frac{K}{\pi}} \varphi_r \rightarrow \phi$ and $\sqrt{\frac{\pi}{K}} \Pi_r \rightarrow \Pi$, yielding

$$H_{\text{sG}} = \frac{\hbar c}{2} \int dx \left\{ \Pi^2 + (\partial_x \phi)^2 \right\} - \frac{\mu^2}{\beta^2} \int dx \cos(\beta \phi), \quad (8)$$

with the interaction parameter β related to the Luttinger parameter K as

$$\beta = \sqrt{\frac{\pi}{K}}, \quad (9)$$

and with $\mu = \sqrt{2\pi J\rho_0/K}$.

3 Lattice regularized and perturbed conformal Hamiltonians for the sine-Gordon model

In order to make the sine-Gordon theory described by the Hamiltonian (8) well-defined, it is necessary to introduce some regularization scheme. In this section, we discuss two prescriptions that are directly related to the TWA and TCSA methods. Sec. 3.1 is devoted to reviewing the lattice regularization of the model, while in Sec. 3.2 the theory is formulated as the relevant perturbation of a massless bosonic conformal field theory. The parameters entering the two different formulations are matched later in Sec. 4, after a description of the TWA and TCSA approaches.

3.1 Lattice regularization

The first regularization uses a spatial discretization by a lattice with spacing a . To keep a direct connection with the cold atomic system we use parameters and variables corresponding to Eq. (7). Denoting $\varphi = \varphi_r$, the lattice regularization of H_r in (7) can be written as

$$H_{\text{Lat}} = \frac{\hbar c}{2} \sum_{j=1}^{N_s} \left(\frac{\pi}{Ka} n_j^2 + \frac{K}{\pi a} (\varphi_j - \varphi_{j-1})^2 \right) - 2J\rho_0 a \sum_{j=1}^{N_s} \cos \varphi_j, \quad (10)$$

where

$$n_k = \frac{Ka}{\pi c} \dot{\varphi}_k, \quad [\varphi_j, n_k] = i\delta_{jk}.$$

The number of sites is given by $N_s = L/a$ and periodic boundary conditions are assumed. This scheme is natural in view of the original microscopic Hamiltonian (4), as the bosonisation formula (6) is written in terms of a coarse grained density and phase, resulting in an effective long wave

length description valid above a short-distance cut-off, the so-called healing length (see Appendix A). In the non-interacting case $J = 0$ the spectrum of the lattice Hamiltonian (10) can be expressed as

$$\varepsilon_k = \frac{2\hbar c}{a} \left| \sin \frac{ka}{2} \right|, \quad (11)$$

reducing to the linear spectrum $\varepsilon_k = \hbar ck$ of a Luttinger liquid for small wave numbers $k \ll 1/a$.

Notice that the cosine term in (10) is not normal ordered. To treat it semiclassically, normal ordering with respect to the bosonic vacuum is necessary. As shown in App. B, this amounts to an additional prefactor

$$\cos \varphi_i = \mathcal{N} : \cos \varphi_i :, \quad (12)$$

with

$$\mathcal{N} = \exp \left(-\frac{\pi \Delta}{N_s} \right) \prod_{n=1}^{N_s/2-1} \exp \left(-\frac{2\pi \Delta}{N_s \sin \frac{\pi n}{N_s}} \right), \quad (13)$$

where

$$\Delta = \frac{1}{8K} = \frac{\beta^2}{8\pi}. \quad (14)$$

The lattice regularization of the Hamiltonian (7) finally takes the form

$$H_{\text{Lat}} = \frac{\hbar c}{2} \sum_i \left(\frac{\pi}{Ka} n_i^2 + \frac{K}{\pi a} (\varphi_i - \varphi_{i-1})^2 \right) - 2J\rho_0 a \mathcal{N} \sum_i : \cos \varphi_i :. \quad (15)$$

3.2 Perturbed conformal field theory formulation

A paradigmatic approach to a massive quantum field theory is to regard it as a perturbation of an ultra-violet (UV) conformal field theory (CFT) [45] with appropriate relevant operators. In this terminology, perturbation does not mean that the coupling is considered to be weak. Rather, it is understood as a deformation of the conformal field theory. Indeed, in models with one space dimension, there exist powerful non-perturbative methods which allow for the treatment of these models at strong coupling as well. In this subsection we use the usual convention of conformal field theory, and work in units $\hbar = 1$ and $c = 1$.

For the sine-Gordon model the corresponding description treats (8) as a compactified massless bosonic conformal field theory, perturbed by the relevant operator $\int dx : \cos \beta \phi :$, where compactification of the bosonic field ϕ means that it takes values on a circle with the identification $\phi \equiv \phi + m \frac{2\pi}{\beta}$, and space-time has a cylindrical geometry due to periodic boundary conditions (PBC) $x \equiv x + L$. Then the perturbed conformal Hamiltonian H_{PCFT} reads

$$H_{\text{PCFT}} = \int_0^L dx \frac{1}{2} : (\partial_t \phi)^2 + (\partial_x \phi)^2 : - \frac{\lambda}{2} \int_0^L dx \left(V_1^{\text{cyl}} + V_{-1}^{\text{cyl}} \right), \quad (16)$$

where the exponential fields

$$V_n^{\text{cyl}} =: e^{in\beta\phi} :^{\text{cyl}} \quad (17)$$

are called vertex operators, and the semicolon denotes normal ordering with respect to the massless scalar field modes. The upper index “cyl” of the normal ordering indicates that these vertex operators have a canonical CFT normalization specified below in (19), and acquire an anomalous dimension. As a result, the coupling λ in the Hamiltonian (16) has a nontrivial dimension related to the scaling exponent Δ (14). Integrability allows to determine its exact relation to the mass gap [46]:

$$\lambda = \left(2 \sin \frac{\xi\pi}{2}\right)^{2\Delta-2} \frac{2\Gamma(\Delta)}{\pi\Gamma(1-\Delta)} \left(\frac{\sqrt{\pi}\Gamma\left(\frac{1}{2-2\Delta}\right)m_1}{2\Gamma\left(\frac{\Delta}{2-2\Delta}\right)}\right)^{2-2\Delta} \quad \text{with} \quad \xi = \frac{\beta^2}{8\pi - \beta^2}, \quad (18)$$

where m_1 is the mass of the first breather in the spectrum sine-Gordon QFT, which is the lightest neutral excitation in the attractive regime¹ i.e. for $\beta^2 < 4\pi$. Relation (18) allows one to express all physical quantities in units of appropriate powers of the first breather mass m_1 .

Following the usual CFT procedure, the theory is continued analytically to imaginary time $\tau = -it$, and we introduce complex coordinates $w = \tau - ix$, $\bar{w} = \tau + ix$ on the resulting Euclidean space-time cylinder. The normalization of the vertex operators is then specified by the following short distance behavior of their two-point functions:

$$\langle 0|V_n^{\text{cyl}}(w_1, \bar{w}_1)V_m^{\text{cyl}}(w_2, \bar{w}_2)|0\rangle = \frac{\delta_{n,-m}}{|w_1 - w_2|^{4n^2\Delta}} + \text{subleading terms}. \quad (19)$$

This shows explicitly that the vertex operators V_n^{cyl} have dimensions of $(\text{length})^{-2n^2\Delta}$, which in units $\hbar = 1 = c$ is the same as $(\text{energy})^{2n^2\Delta}$ or $(\text{mass})^{2n^2\Delta}$.

As a next step, the conformal transformation $z = \exp\frac{2\pi}{L}w$ maps the cylinder to the complex plane parametrized by the dimensionless complex coordinates z and \bar{z} . Under this transformation, the vertex operators $V_{\pm 1}$ transform as conformal primary fields of left/right weights (Δ, Δ) [45]:

$$V_{\pm 1}^{\text{pl}}(z, \bar{z}) \left(|z| \frac{2\pi}{L}\right)^{2\Delta} = V_{\pm 1}^{\text{cyl}}(w, \bar{w}), \quad (20)$$

where unlike the vertex operators V^{cyl} defined on the cylinder, vertex operators V^{pl} defined on the plane are dimensionless. Hence (20) allows to express (16) as²

$$H_{\text{PCFT}} = \frac{2\pi}{L} \left(L_0 + \bar{L}_0 - \frac{1}{12}\right) - \lambda \left(\frac{2\pi}{L}\right)^{2\Delta} \frac{L}{2} \int_0^{2\pi} \frac{d\vartheta}{2\pi} \left[V_{+1}^{\text{pl}}(e^{i\vartheta}, e^{-i\vartheta}) + V_{-1}^{\text{pl}}(e^{i\vartheta}, e^{-i\vartheta})\right], \quad (21)$$

i.e. in terms of a dimensionless cosine operator $(V_{+1}^{\text{pl}} + V_{-1}^{\text{pl}})/2$, which can be straightforwardly matched to the corresponding operator $:\cos\varphi_i:$ in the lattice regularized approach. Note that any two definitions of the exponential operator are related by some multiplicative renormalisation using the Baker-Campbell-Hausdorff formula (77). Operators $(V_{+1}^{\text{pl}} + V_{-1}^{\text{pl}})/2$ and $:\cos\varphi_i:$ have identical normalization since they both have expectation value 1 in the vacuum state of the massless free boson defined by setting $\lambda = 0$ in the PCFT and $J = 0$ on the lattice. A similar result is true for the relation between the sine operators.

¹In the repulsive regime $4\pi \leq \beta^2 \leq 8\pi$ the lightest excitations are topologically charged solitons, whose mass is similarly related to λ ; the point $\beta^2 = 8\pi$ corresponds to a Kosterlitz-Thouless transition above which the cosine perturbation becomes irrelevant and the spectrum is gapless.

²The ϑ integral runs over the unit circle as $z = e^{i\vartheta}$, corresponding to $\tau = 0$ on the cylinder.

The first part of the Hamiltonian (21) involves the generators L_0 and \bar{L}_0 of the Virasoro algebra and is just the free massless boson Hamiltonian in finite volume, which can be rewritten in terms of the usual bosonic operators as

$$H_{\text{CFT}} = \frac{2\pi}{L} \left(\pi_0^2 + \sum_{k>0} a_{-k} a_k + \sum_{k>0} \bar{a}_{-k} \bar{a}_k - \frac{1}{12} \right), \quad (22)$$

with

$$\begin{aligned} [\phi_0, \pi_0] &= i & [a_k, a_l] &= k\delta_{k+l} \\ [\bar{a}_k, \bar{a}_l] &= k\delta_{k+l}, \end{aligned} \quad (23)$$

where ϕ_0 and π_0 are the zero mode of the canonical field and its conjugate momentum. The operators a_k and \bar{a}_k correspond to right and left oscillator modes creating/annihilating particles with momentum $p = \pm 2\pi|k|/L$.

The Hilbert space \mathcal{H} is composed of Fock modules \mathcal{F}_n , built upon Fock vacua $|n\rangle = V_n(z=0)|0\rangle$ using the oscillator modes, and its basis is given as

$$a_{-k_1} \dots a_{-k_r} \bar{a}_{-p_1} \dots \bar{a}_{-p_l} |n\rangle : n \in \mathbb{Z}, r, l \in \mathbb{N}, k_i, p_j \in \frac{2\pi}{L} \mathbb{N}^+, \quad (24)$$

which are eigenstates of H_{CFT} with energy

$$E = \frac{2\pi}{L} \left(\frac{(n\beta)^2}{4\pi} + \sum_{i=1}^r k_i + \sum_{j=1}^l p_j - \frac{1}{12} \right). \quad (25)$$

The ground state of the conformal field theory is the Fock vacuum with $n = 0$, i.e. $|0\rangle$.

Note that the PCFT Hamiltonian is obtained by setting (Euclidean) time to $\tau = 0$. In the subsequent calculations we use this Hamiltonian for time evolution, which means that we use a Schrödinger picture in which operators are time-independent and states evolve under the full Hamiltonian in contrast with the usual conformal field theory picture, where the operators are evolved by the conformal Hamiltonian (22). The two pictures are physically equivalent via a similarity transformation by the operator

$$e^{-\tau H_{\text{CFT}}}.$$

Finally, it is useful to measure all quantities in units of the first breather mass m_1 , and define a dimensionless volume variable as

$$l = m_1 L. \quad (26)$$

This normalization implies that distance is measured in units of the Compton wave length corresponding to the first breather:

$$\ell_1 = \frac{\hbar}{m_1 c}. \quad (27)$$

4 How TWA and TCSA work

This section treats the methods used to simulate the time evolution: first the truncated Wigner approximation in Sec. 4.1, then the truncated conformal space approach Sec. 4.2, and then describes the parameter matching between the two approaches in Sec. 4.3.

4.1 Truncated Wigner approximation

The truncated Wigner approximation (TWA) is a powerful semiclassical method. It is constructed through a systematic expansion of the Keldysh path integral [32, 33] and is well suited for calculating out-of-equilibrium expectation values and correlations. In this section we present the TWA formulas for the lattice Hamiltonian (10), while for the sake of completeness we review the detailed derivation of the method in App. D following Refs. [32, 33].

Our main purpose here is the calculation of the out-of-equilibrium expectation value $\langle \hat{\mathcal{O}} \rangle(t)$ of an arbitrary operator $\hat{\mathcal{O}}$, for an initial state given by the density matrix $\hat{\rho}_0$, and a time evolution governed by the Hamiltonian (10). First we introduce the notations $|\varphi\rangle_j$ and $|n\rangle_j$ for the eigenstates of the operators $\hat{\varphi}_j$ and \hat{n}_j , respectively. These eigenstates satisfy the completeness relations

$$\mathbb{I}_j = \int_{-\pi}^{\pi} \frac{d\varphi}{2\pi} |\varphi\rangle_j \langle \varphi| = \sum_{n \in \mathbb{Z}} |n\rangle_j \langle n| \quad (28)$$

at any site j , while their overlap is given by

$${}_j \langle \varphi | n \rangle_j = e^{i\varphi n}. \quad (29)$$

Relying on the observation that the phase never winds by the full period 2π in our simulations, in the following we neglect the 2π periodicity of the phase, which would ensure that the particle number operator takes integer values. In this approximation both φ and n become continuous variables, and the completeness relation (28) is replaced by

$$\mathbb{I}_j = \int_{-\infty}^{\infty} \frac{d\varphi}{2\pi} |\varphi\rangle_j \langle \varphi| = \int_{-\infty}^{\infty} dn |n\rangle_j \langle n|. \quad (30)$$

Below we will use a more compact vector notation

$$\underline{\varphi} = \{\varphi_j | j = 1, \dots, N_s\} \quad (31)$$

for the full set of eigenvalues, with analogous notation for the eigenvalues of the particle number operators \hat{n}_j .

In the TWA we express the expectation value $\langle \hat{\mathcal{O}} \rangle(t)$ in terms of the Wigner function of the initial state,

$$W(\underline{\varphi}, \underline{n}) = \frac{1}{(2\pi)^{2N_s}} \int d\underline{\varphi}' \langle \underline{\varphi} + \underline{\varphi}'/2 | \hat{\rho}_0 | \underline{\varphi} - \underline{\varphi}'/2 \rangle e^{-i\underline{\varphi}' \cdot \underline{n}}, \quad (32)$$

with $\hat{\rho}_0$ denoting the density matrix at $t = 0$, and in terms of the Wigner transform of the operator $\hat{\mathcal{O}}$,

$$O_W(\underline{\varphi}, \underline{n}) = \frac{1}{(2\pi)^{N_s}} \int d\underline{\varphi}' \langle \underline{\varphi} - \underline{\varphi}'/2 | \hat{\mathcal{O}} | \underline{\varphi} + \underline{\varphi}'/2 \rangle e^{i\underline{\varphi}' \cdot \underline{n}}. \quad (33)$$

The resulting TWA expression can be written in a compact form as

$$\langle \hat{\mathcal{O}} \rangle_{\text{TW}}(t) = \int \int d\underline{\varphi} d\underline{n}_0 W(\underline{\varphi}_0, \underline{n}_0) O_W(\underline{\varphi}(t), \underline{n}(t)), \quad (34)$$

where the components of the trajectories $\underline{\varphi}(t')$ and $\underline{n}(t')$ are determined by the following classical equations of motion,

$$\begin{aligned} \partial_t n_j &= -\frac{Kc}{\pi a} (\varphi_{j+1} + \varphi_{j-1} - 2\varphi_j) - \frac{2J\rho_0 a}{\hbar} \sin \varphi_j, \\ \partial_t \varphi_j &= \frac{c\pi}{Ka} n_j, \end{aligned} \quad (35)$$

solved for initial conditions $\{\underline{\varphi}_0, \underline{n}_0\}$ (see App. D.1 for more details).

Using the TWA result (34), the time evolution of observables can be evaluated by the following procedure. We generate random initial conditions $\{\underline{\varphi}_0, \underline{n}_0\}$, drawn from the distribution given by the initial Wigner function $W(\underline{\varphi}_0, \underline{n}_0)$, and we obtain the classical trajectories from (35). Substituting the fields $\underline{\varphi}(t)$ and $\underline{n}(t)$ into the Wigner transform O_W gives a single realization of the observable. The TWA expectation value (34) of the observable at time t is then evaluated as the average of $O_W(\underline{\varphi}(t), \underline{n}(t))$ over realizations corresponding to a large number of different initial conditions.

As already mentioned at the beginning of this section, the TWA arises as the leading order contribution of a systematic expansion of the Keldysh path integral in terms of quantum fields (see App. D.1). In the App. D.2 we also examine the next term of this expansion, and compare the resulting quantum correction to the TWA result, Eq. (34).

4.2 Truncated conformal space approach

The truncated conformal space approach (TCSA) is an efficient numerical method to study perturbed conformal field theories, originally introduced in [34]. The main idea is to consider the theory of interest in a finite volume L resulting in a discrete spectrum of the unperturbed CFT, which can be truncated to a finite subspace by introducing an upper energy cut-off parameter e_{cut} . For many perturbations of CFTs it is possible to calculate exact matrix elements of the perturbing field and various operators in the truncated Hilbert space. Therefore, computing the spectrum of the perturbed theory and other physical quantities reduces to manipulations with finite dimensional matrices.

For the sine-Gordon TCSA [47] the starting point is the Hamiltonian (21) of a compactified free massless boson in finite volume L , perturbed by a relevant cosine operator with the Hilbert space in finite volume spanned by the basis (24). Using the simplest truncation scheme described above, the truncated space is given by

$$\mathcal{H}_{\text{TCSA}}(e_{\text{cut}}) = \text{span} \left\{ a_{-k_1} \dots a_{-k_r} \bar{a}_{-p_1} \dots \bar{a}_{-p_l} |n\rangle : \frac{(n\beta)^2}{4\pi} + \sum_{i=1}^r k_i + \sum_{j=1}^l p_j - \frac{1}{12} \leq e_{\text{cut}} \right\} \quad (36)$$

which is the scheme commonly employed in the literature. To keep our notations compact, we return to the conformal field theoretical convention $\hbar = 1$ and $c = 1$ in this section.

In our investigations of the time evolution it is more convenient to use a different truncation scheme with two parameters. The number of Fock modules is fixed by requiring $|n| \leq n_{\text{cut}}$, but within each module we also apply a module independent energy cut-off e_{cut} . This prescription leads to the following truncated Hilbert space:

$$\mathcal{H}_{\text{TCSA}}(e_{\text{cut}}, n_{\text{cut}}) = \text{span} \left\{ a_{-k_1} \dots a_{-k_r} \bar{a}_{-p_1} \dots \bar{a}_{-p_l} |n\rangle : \sum_{i=1}^r k_i + \sum_{j=1}^l p_j \leq e_{\text{cut}}, |n| \leq n_{\text{cut}} \right\}. \quad (37)$$

The effect of the in-module energy cut-off e_{cut} can partially be eliminated using ideas inspired by the renormalisation group as discussed in App. C in more detail. There are no analogous methods to compensate the effect of the other truncation parameter n_{cut} , so we chose an alternative approach. For the time evolution of a state, one can choose a suitable fixed value of n_{cut} by requiring that the norm of the component of the time evolved state falls inside the extremal Fock modules remain small for the time period considered in the simulation. This condition can be easily checked during the numerical time evolution. Although the calculation of expectation values of operators with respect

number asymmetry only decrease in proportion to the total particle number, but not in absolute magnitude. Of course l can also be decreased to reduce the fluctuations; however, smaller volume not only decreases the upper time limit accessible by the TCSA evolution, but for values $l \lesssim 10$ (i.e. $L \lesssim 10\ell_1$ with the Compton length $\ell_1 = \hbar/(m_1c)$) setting the correlation length $\xi_{\text{corr}} \approx \ell_1$), one expects strong finite size corrections to the infinite volume sine-Gordon dynamics.

4.3 Parameter matching

The sine-Gordon theory has a natural correlation length ξ_{corr} which can be identified as the Compton wave length ℓ_1 given in Eq. (27). To compare results in the lattice and perturbed conformal field theory formulation, ξ_{corr} must be larger than the lattice spacing. Since we also compare dynamical quantities, it is also necessary that the lattice regularized dispersion relation (11) be linear in the energy range influencing the dynamics. Given these conditions, the only remaining task is to express the dimensionless volume parameter l of the PCFT, Eq. (26), in terms of the lattice parameters, since the only other parameter of the QFT β is already expressed in terms of the Luttinger parameter K in (9). In this section we restore \hbar and c explicitly to obtain the relations in terms of the physical units used in the experiments. It is then convenient to introduce the dimensionless coupling κ by rewriting (18) in the form $\lambda/(\hbar c) = \kappa \ell_1^{2\Delta-2}$. Using (15) and (21) we obtain the relation

$$\kappa \ell_1^{2\Delta-2} \left(\frac{2\pi}{L} \right)^{2\Delta} = \frac{2J\rho_0}{\hbar c} \mathcal{N}. \quad (41)$$

From these relations the mass of the first breather in the field theory is expressed in terms of the lattice quantities as

$$m_1 = \frac{\hbar}{c} \left(\frac{2J\rho_0}{\kappa\hbar c} \mathcal{N} \left(\frac{L}{2\pi} \right)^{2\Delta} \right)^{\frac{1}{2-2\Delta}}, \quad (42)$$

and the dimensionless volume turns out to be

$$l = L/\ell_1 = \left(\frac{JLN\mathcal{N}}{\kappa\hbar c(2\pi)^{2\Delta}} \right)^{\frac{1}{2-2\Delta}}. \quad (43)$$

To compare dynamical quantities we recall that in lattice simulations it is customary to measure time in units of the (bare/unrenormalized) Josephson time $T_J = 1/f_J$ with

$$f_J = \sqrt{\frac{J}{\hbar} \frac{c}{2KL} N}. \quad (44)$$

Here f_J arises as the oscillation frequency in the single mode approximation of the lattice Hamiltonian (10), with homogeneous phase and particle number difference $\varphi_j \equiv \varphi_0$ and $n_j \equiv n_0$,

$$H_{\text{sing.m.}} = \frac{\hbar c\pi}{2KL} n_0^2 - 2J\rho_0 L \cos \varphi_0 \quad (45)$$

within the harmonic approximation $\cos \varphi_0 \approx 1 - \varphi_0^2/2$. Note that $H_{\text{sing.m.}}$ coincides with the pendulum considered in the introduction with the identification $U = \hbar c\pi/(2KL)$. On the other hand, in the QFT the convenient dimensionless variable is $\nu_1 t$, with the frequency ν_1 associated with the breather mass,

$$\nu_1 = \frac{m_1 c^2}{\hbar}. \quad (46)$$

It is then easy to calculate the relation between the dimensionless times $f_J t_{\text{Lat}}$ and $\nu_1 t_{\text{QFT}}$ and eventually between f_J and ν_1 from (43), (44) and (46) yielding

$$f_J = \frac{\nu_1}{\chi}. \quad (47)$$

Here

$$\chi = \left(\frac{l}{2\pi}\right)^\Delta \frac{1}{\beta} \sqrt{\frac{\mathcal{N}}{\kappa}}, \quad (48)$$

in which χ is expressed in terms of the QFT quantities β and $l = L/\ell_1$, and the number of lattice sites N_s , but can also be easily recast in terms of the parameters of the lattice Hamiltonian (15).

5 Simulations

In this section, we focus on two different initial states, and study their time evolutions using the TWA and TCSA methods. In order to test the methods both in and out of the regime of classical self-trapping of the simplified pendulum model (1), we consider initial states with finite and zero particle number imbalance. For technical reasons, TCSA can not treat initial states intersecting the separatrix, since a state having finite weight in both phases quickly spreads into a large number of Fock modules. We note that the validity of TWA is also questionable in the vicinity of the phase boundary, because here the trajectories are very sensitive to small perturbations, which is expected to result in a large quantum correction to the TWA.

First we consider two identical condensates with zero particle number imbalance in Sec. 5.1; here the relevant trajectories are not self-trapped. We then impose a large enough initial particle number difference in Sec. 5.2 so that the trajectory lies deep in the self-trapped phase.

5.1 Two independent and identical condensates in their ground state

First we consider an initial state with two identical condensates in their ground states and well-defined atom numbers $N/2$ on each side. In principle, one could reach this state by first cooling the atoms in the presence of a high barrier, and then coupling them by decreasing the barrier height to establish Josephson tunneling. In practice, a similar state can be implemented experimentally by first raising adiabatically the barrier between the condensates and then waiting until they decohere. In the latter case, however, the initial state would display large atom number fluctuations on each side.

In this setup, the phases of the two condensates are initially uncorrelated, and therefore $\langle \cos \varphi(x) \rangle = 0$ at any point x at time $t = 0$. Tunneling, however, leads to a build-up of phase correlations, and gives rise to a non-zero expectation value, $\langle \cos \varphi(x) \rangle \neq 0$. This phenomenon is called phase locking. Notice that while the global (average) phases may become almost perfectly correlated, the value of $\langle \cos \varphi \rangle$ is always reduced by quantum fluctuations and fluctuations due to the finite energy density of excitations after the quench. Therefore, even for strong phase locking, $\langle \cos \varphi \rangle \lesssim 1$. In this initial state, the difference $N_L - N_R$ between left and right particle numbers vanishes at $t = 0$, and its expectation value also remains zero at all times. Notice that – due to the periodic boundary conditions – one-point functions of local operators are position independent.

The initial state above can be implemented easily with both methods. Within TCSA, the initial state corresponds simply to the ground state of the unperturbed free boson CFT, while within TWA, it is described by the Wigner function

$$W = \frac{\theta(\varphi_0 + \pi)\theta(\pi - \varphi_0)}{2\pi} \delta_{n_0,0} \prod_{k>0} \frac{4}{\pi^2} \exp\left(-\sigma_k^2 \varphi_k \varphi_{-k} - \frac{4 n_k n_{-k}}{\sigma_k^2}\right), \quad (49)$$

with $\varphi_0 = \sum_{j=1}^{N_s} \varphi_j / N_s$ the global phase difference, $n_0 = \sum_{j=1}^{N_s} n_j$ the difference of atom numbers, and $n_{k \neq 0}$ and $\varphi_{k \neq 0}$ the standard Fourier coefficients,

$$n_{k \neq 0} = \frac{1}{\sqrt{N_s}} \sum_{j=1}^{N_s} e^{-ikja} n_j, \quad \varphi_{k \neq 0} = \frac{1}{\sqrt{N_s}} \sum_{j=1}^{N_s} e^{-ikja} \varphi_j. \quad (50)$$

The particle number difference n_0 takes on the well defined value $n_0 = 0$, while the global relative phase φ_0 is completely random in the interval $(-\pi, \pi)$. The variance σ_k^2 is determined by zero-point fluctuations, and is given by

$$\sigma_k^2 = \frac{4K}{\pi} \sin \frac{ka}{2} \approx \frac{2Kka}{\pi}, \quad (51)$$

with the last approximation valid in the regime of linear spectrum, where $\varepsilon_k \approx \hbar ck$.

Fig. 2.a displays the time evolution of $\cos \varphi$ as computed by TWA, and the corresponding quantity $\mathcal{N} \langle : \cos \beta \phi : \rangle^{\text{pl}}$ computed by TCSA, with the upper index ‘‘pl’’ referring to the PCFT expectation value calculated on the (z, \bar{z}) complex plane, as discussed in Sec. 3.2. Note that the expectation value of the cosine operator calculated on the plane can be easily expressed by that of defined on the cylinder as $\langle : \cos \beta \phi : \rangle^{\text{pl}} = \left(\frac{L}{2\pi}\right)^{2\Delta} \langle : \cos \beta \phi : \rangle^{\text{cy}}$ according to (20). The time evolution of the standard deviation of the asymmetry between the number of atoms in the right and left condensates

$$\frac{\hat{N}_R - \hat{N}_L}{2} = \sum_{j=1}^{N_s} \hat{n}_j \quad (52)$$

is presented in Fig. 2.b. Within TCSA, this variable corresponds to the quantum number n labelling the Fock modules \mathcal{F}_n .³

The TWA results are plotted against the unrenormalized Josephson frequency, f_J , Eq. (44), while TCSA data are presented in terms of the frequency associated with the first breather ν_1 , Eq. (46), corresponding to a renormalized Josephson frequency. Notice that the time needs only a $\sim 30\%$ rescaling, signaling that even for the strong interactions corresponding to the system analyzed in Fig. 2, renormalisation effects are sizable but not crucial for the experimentally relevant system sizes.

The TCSA curves were obtained by implementing a renormalisation group-based extrapolation, outlined in App. C, using the raw results with energy cut-offs $e_{cut} = 12, 14, 16$ and 18 as input. The other TCSA truncation parameter n_{cut} was set to 11 , which ensured that the norm of the component of the time evolved state in the extremal Fock modules \mathcal{F}_{11} and \mathcal{F}_{-11} remained smaller than 10^{-3} for the time range considered.

³This is also apparent from the block-diagonal form of the Hamiltonian (40) since the blocks $\mathcal{V}_{\pm 1}$ change n by ± 1 , while according to the bozonization relations (6) they correspond to the tunneling of an atom from the left to the right and vice versa, respectively, described by the two terms in Eq. (4).

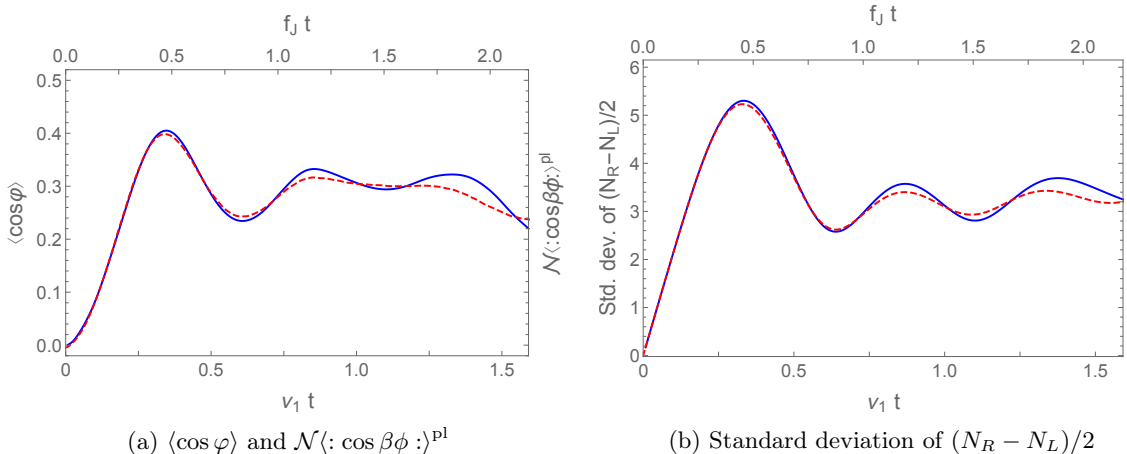


Figure 2: Time dependent expectation value of (a) $\cos \varphi$ and $\mathcal{N} \langle \cos \beta \phi \rangle^{\text{pl}}$ and (b) the standard deviation of half of the particle number difference. Continuous blue curves correspond to extrapolated TCSA data, while dashed red lines to TWA. For TWA we have used $K = 1.56$, $L = 14.86 \mu\text{m}$, $N = 400$, $c = 2800 \mu\text{m/s}$, $J/h = 7\text{Hz}$ and $N_s = 60$, corresponding to a Josephson frequency $f_J = 410.8\text{Hz}$. The parameters of TCSA are $\beta = 1.42$, $\nu_1 = 299.8\text{Hz}$, and the dimensionless length $l = 10$. Time evolution is measured in terms of the bare Josephson frequency f_J (TWA) and the renormalized Josephson frequency, corresponding to the frequency associated with the first breather, i.e. ν_1 (within TCSA). Here and in all subsequent figures the upper index “pl” indicates the PCFT expectation value computed on the (z, \bar{z}) complex plane as specified in Sec. 3.2.

The numerical results obtained by the two methods show good agreement within the accessible time frame. Estimating the errors of the two numerical methods is a rather involved task, which deserves some attention. For the TCSA, one can get an idea about the order of magnitude of the remaining truncation errors by investigating the cut-off dependence of extrapolated curves. Since we have only order-of-magnitude estimates, we chose not to indicate them directly in Fig. 2, but they remain rather small on the scale of the plots.

For the TWA, errors turn out to be much less controlled: we have estimated quantum corrections by examining the next terms in the semiclassical expansion of the Keldysh action and found that these become sizable in a rather short time (see App. D.2). On the other hand, the very good agreement with TCSA suggests that the *actual* error is much smaller than our estimate, and can be crudely estimated by the deviation between the two simulation results. We thus do not have at present a good way to control the accuracy of TWA, which nevertheless performs in this case surprisingly well.

The results presented in this subsection appear to disagree with those of recent experiments, which reported a rapid build-up of partial phase coherence between the condensates, followed by a somewhat slower relaxation to a phase-locked steady state with $\langle \cos \varphi \rangle \approx 1$ [17]. Instead, here we find that $\langle \cos \varphi \rangle$ quickly approaches a stationary value considerably lower than 1 for the sine-Gordon model. Even though the experiments of the Schmiedmayer group were performed on a weakly interacting system, while our results in Fig. 2 have been obtained for a Luttinger parameter $K = 1.56$, corresponding to strong atom-atom interactions, we would observe a similar stationary value for weaker interactions. We return to a more detailed discussion of this issue in the conclusions.

5.2 Two condensates in their ground state with a particle number difference

We now turn to the investigation of the regime of classical self-trapping. To this end we discuss the situation where the two condensates are prepared in their ground states, but with a large enough initial particle number asymmetry, $(N_R - N_L)/2 = N_0$, such that the initial state is far enough from the separatrix as shown in Fig. 1. (In practice, we monitor the number of relevant Fock modules in TCSA, and we ensure that the state does not leak into the non-trapped phase during the time evolution.) In TCSA, this state is the ground state $|N_0\rangle$ of the Fock-module \mathcal{F}_{N_0} , while in the TWA it corresponds to the Wigner function (49), but with the factor $\delta_{n_0,0}$ replaced by δ_{n_0,N_0} . The evolution of the expectation values of the cosine and the sine of the relative phase are presented in Fig. 3, while the expectation value and standard deviation of the particle number difference are shown in Fig. 4. Note that unlike in the previous setting, the sine of the phase and the particle number asymmetry are both non-vanishing due to the asymmetry in the initial state.

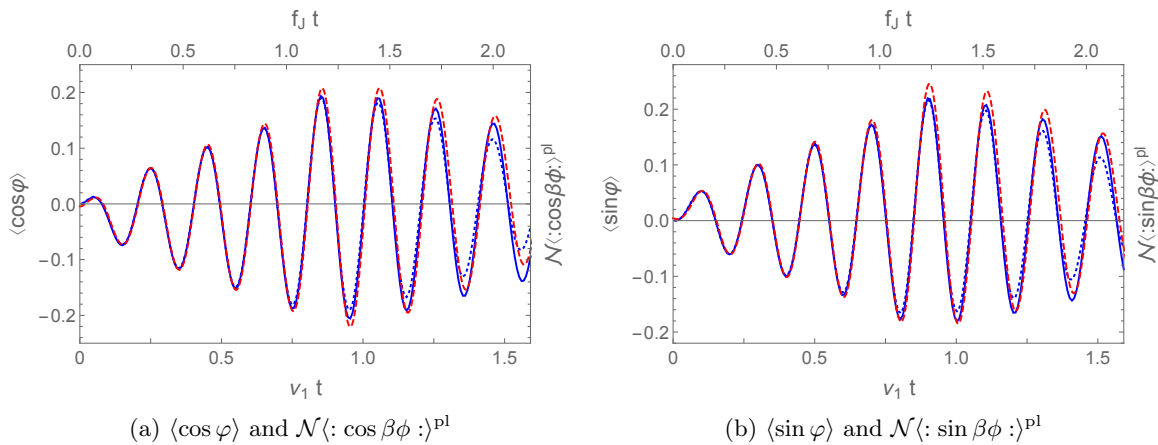


Figure 3: Comparing results for (a) $\cos \varphi$ and $\mathcal{N} : \cos \beta \phi :^{\text{pl}}$, and (b) $\sin \varphi$ and $\mathcal{N} : \sin \beta \phi :^{\text{pl}}$, obtained from TWA and TCSA, respectively. Blue continuous curve corresponds to TCSA with $e_{\text{cut}} = 18$, blue dotted curve to the extrapolated TCSA data and red dashed curve to TWA, for an initial particle number imbalance $(N_R - N_L)/2 = 25$. The parameters of TWA are $K = 1.56$, $L = 14.86 \mu\text{m}$, $N = 400$, $c = 2800 \mu\text{m/s}$, $J/h = 7\text{Hz}$ and $N_s = 60$, corresponding to a Josephson frequency $f_J = 410.8\text{Hz}$. For TCSA we used $\beta = 1.42$, $\nu_1 = 299.8\text{Hz}$, and the dimensionless length $l = 10$. Time evolution is measured in terms of the bare (TWA) and renormalized (TCSA) Josephson frequency, f_J and ν_1 , respectively.

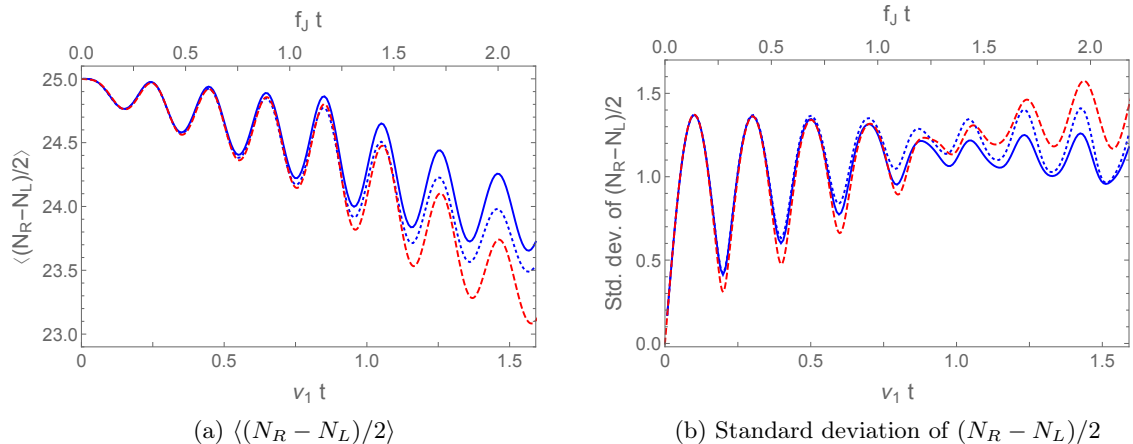


Figure 4: Time dependent expectation value of half of the particle number difference (a) and its standard deviation (b), for an initial particle number imbalance $(N_R - N_L)/2 = 25$, with blue continuous, blue dotted and red dashed curves corresponding to TCSA with $e_{\text{cut}} = 18$, to the extrapolated TCSA data and to TWA, respectively. The parameters of TWA are $K = 1.56$, $L = 14.86 \mu\text{m}$, $N = 400$, $c = 2800 \mu\text{m/s}$, $J/h = 7\text{Hz}$ and $N_s = 60$, corresponding to a Josephson frequency $f_J = 410.8\text{Hz}$. For TCSA we used $\beta = 1.42$, $\nu_1 = 299.8\text{Hz}$, and the dimensionless length $l = 10$. Time is measured in units of the bare (TWA) and renormalized (TCSA) Josephson frequency, f_J and ν_1 , respectively.

For the one point functions $\cos \varphi$ and $\sin \varphi$ the match between the TCSA and TWA is excellent when considering the blue continuous curve (corresponding to TCSA with $e_{\text{cut}} = 18$) and the red dashed curve (TWA). However, the TCSA extrapolation drives away the curves for slightly larger times. In contrast, for the standard deviation of $(N_R - N_L)/2$ and especially for its average, the extrapolation results in better agreement. This is due to the initial state being highly excited, resulting in a larger extrapolation error for the available values of the cut-off (see App. C), which is also manifested in the quality of the individual extrapolation fits. Therefore it is not possible to decide a priori whether the extrapolated curve or the one with the highest energy cut-off is closer to the correct PCFT result. However, this uncertainty is negligible for shorter times, therefore in this regime the sine-Gordon time evolution is captured correctly both by the TWA and the TCSA.

For the TCSA extrapolation in energy, runs with cut-off values $e_{\text{cut}} = 12, 14, 16$ and 18 were used. In addition, for all the TCSA simulations $n_{\text{cut}} = 11$ was chosen, which means that Fock-modules \mathcal{F}_n from the range $n_0 - n_{\text{cut}} \leq n \leq n_0 + n_{\text{cut}}$ (i.e. $\mathcal{F}_{14}, \dots, \mathcal{F}_{36}$) were included in the truncated Hilbert space. With this choice, the square of the norm of the time evolved state remained less than 10^{-7} in the extremal Fock modules \mathcal{F}_{14} and \mathcal{F}_{36} during the entire time evolution.

All one-point functions displayed in Figs. 3 and 4 show pronounced oscillations with a period T much smaller than the bare Josephson time T_J ,

$$T/T_J \approx 0.3. \quad (53)$$

We can understand these faster oscillations by considering the classical trajectories of the pendulum (1). The period of the trajectory of energy E is given by

$$T_E = \oint \frac{d\varphi_0}{\dot{\varphi}_0} = \hbar \oint \frac{d\varphi_0}{2Un_0} = \frac{\hbar}{2\sqrt{U}} \oint \frac{d\varphi_0}{\sqrt{E + NJ \cos \varphi_0}}, \quad (54)$$

with the integral running along the trajectory. With the parametrization of Eq. (1), the bare Josephson time, the period corresponding to the lowest energy $E_0 = -JN$, is given by

$$T_J = \frac{h}{\sqrt{2UNJ}}. \quad (55)$$

Comparing T_J to the period of a self-trapped trajectory, we arrive at

$$\frac{T_E}{T_J} = \frac{\sqrt{2}}{\pi\sqrt{1+E/(NJ)}} \left\{ F\left(\frac{\pi}{2} \middle| \frac{2}{1+E/(NJ)}\right) - F\left(-\frac{\pi}{2} \middle| \frac{2}{1+E/(NJ)}\right) \right\}, \quad (56)$$

with F denoting the elliptic integral of the first kind. By evaluating this expression for the trajectory touched by our initial state at $\varphi_0 = 0$ (see Fig. 1), corresponding to energy

$$E = \frac{\hbar c\pi}{2KL} N_0^2 - JN, \quad (57)$$

we find $T_E/T_J = 0.3$, in excellent agreement with the numerics.

Moreover, the expectation values plotted in Fig. 3 show a pronounced beating. This effect can be qualitatively understood by noting that the classical trajectories intersected by the initial state fall in a small frequency window, and the dominant contribution to the dynamics comes from the vicinity of the trajectories touched at $\varphi_0 = 0$ and $\varphi = \pi$ (see Fig. 1). The period of the beating can be estimated from the frequency shift between these two trajectories, leading to

$$1/T_b = 1/T_{E_1} - 1/T_{E_2} \quad (58)$$

with

$$E_{1,2} = \frac{\hbar c\pi}{2KL} N_0^2 \pm JN. \quad (59)$$

These considerations result in the estimate $T_b/T_J \approx 1.8$, which is by a factor of 1.5 smaller than the beating period observed in the numerics. This discrepancy most likely originates from the presence of $k \neq 0$ modes, oscillating with a frequency slightly shifted compared to the frequency of the zero mode, and strongly renormalizing the period of beating.

We note that the $k \neq 0$ modes also have a pronounced effect on the dynamics of the particle number difference $(N_L - N_R)/2$, plotted in Fig. 4. On the top of oscillations, $(N_L - N_R)/2$ decreases gradually, since the large excitation energy stored in the zero mode in the initial state is transferred to the $k \neq 0$ modes in the course of the time evolution.

6 Conclusions

In this work, we studied real-time out-of-equilibrium time evolution in the quantum sine-Gordon model by comparing the truncated Wigner approximation (TWA) and the truncated conformal space approach (TCSA). Quantum quenches in the sine-Gordon model have received considerable interest recently, especially in light of experiments involving cold atomic gases such as coupled quasi-one-dimensional bosonic condensates [15, 17], in which the effective description of the dynamics is thought to be provided by sine-Gordon theory. Therefore, besides establishing connection between the parametrization of the two numerical methods together with linking these parameters to the experimental ones, we also concentrated on studying quench protocols relevant to experimental investigations.

Whereas the applied numerical approaches are relatively easy to implement, estimating their systematic error and therefore their applicability is a difficult, and for the TWA an essentially

unsolved problem. In the case of the TCSA, the RG-based cut-off extrapolation provides a useful improvement as well as giving an idea of the magnitude of truncation errors from the quality of the cut-off extrapolation fits. The TCSA method is expected to face difficulties for highly excited states which was indeed found to be the case.

For the sine-Gordon TWA, in contrast to TWA based on coherent state representation, no natural small parameter emerges to control the expansion of the Keldysh path integral, and hence neglecting quantum corrections is not guaranteed to capture essential physics. In fact we found that the evaluation of the next quantum correction seriously overestimates the error, and therefore the approximation is largely uncontrolled. Therefore comparison with results obtained by the alternative method of TCSA has a high value, since a good agreement is strong evidence for the reliability of the results.

We have studied two very different initial conditions. In the first case, we assumed two independent condensates, which are then connected by a Josephson tunneling term at time $t = 0$. A quick initial rise of the expectation value of $\langle \cos \varphi \rangle$ has been observed with both methods, which, followed by a few oscillations, leveled off at a value $\langle \cos \varphi \rangle < 1$. The other initial state we have studied assumed a large particle number difference at time $t = 0$. In this second case the system was in the trapped phase and simultaneous beating effects and oscillations appeared.

For the particular parameters of the sine-Gordon model and the quench protocols discussed in the paper, excellent agreement was found between results for time evolved quantities obtained by the two methods for the first few oscillations up to times of order $t/T_J = 2$ with T_J denoting the Josephson time in the model (i.e., the oscillation period within a harmonic single mode approximation for the coupled condensates). In the language of conformal field theory, this time scale corresponds to $c^2 m_1 t / \hbar = 10$, where m_1 is the mass gap, emerging from the first breather in the attractive regime studied here. This demonstrates the time evolution of expectation values are correctly captured by both methods, at least for initial states and the particular parameter range considered here.

In microtraps, the time evolution of the overall phase difference and particle number difference is often described in terms of a simple pendulum model [17]. Just as ordinary pendulums, according to this simple model, the condensate exhibits two characteristically different behaviors, indeed observed experimentally; for small particle number and phase differences it displays Josephson oscillations, while for larger particle number differences a self-trapped motion appears. Here we have tested TWA and TCSA both in the non-trapped and in the self-trapped regimes, by considering two important – and also experimentally relevant – initial states, with two decoupled condensates prepared in their ground states. In the first (symmetrical) case both condensates contained the same number of particles, whereas in the second (asymmetrical) case the difference in their particle numbers was large enough to enter the regime of classical self-trapping⁴. For the symmetrical initial state, we calculated the expectation value of the cosine of the phase of the two condensates and the standard deviation of the particle number difference. In the asymmetrical case these quantities were supplemented by the average of the sine of the phase and the average of the particle number difference itself, which vanish for the first starting condition, but are non-trivial for the second one.

Recent experiments demonstrate that two Josephson-coupled one dimensional condensates show a rapid relaxation to a phase-locked steady state [17] with $\langle \cos \varphi \rangle = 1$. This behavior is very robust against initial conditions and physical parameters, and stands opposed to previous theoretical results [31, 48, 49], as well as to our own findings. In the symmetrical case we found that the phase oscillates yielding values of $\langle \cos \varphi \rangle$ significantly smaller than one, and the curves are consistent with a slow

⁴Using the language of conformal field theory, these states are eigenstates of the free massless bosonic field theory whose perturbation with $:\cos \beta \phi:$ results in the sine-Gordon model. The first case corresponds to the vacuum of the free massless theory, while the second is a similar Gaussian state with a non-zero eigenvalue with respect to the zero mode of the canonical conjugate momentum field.

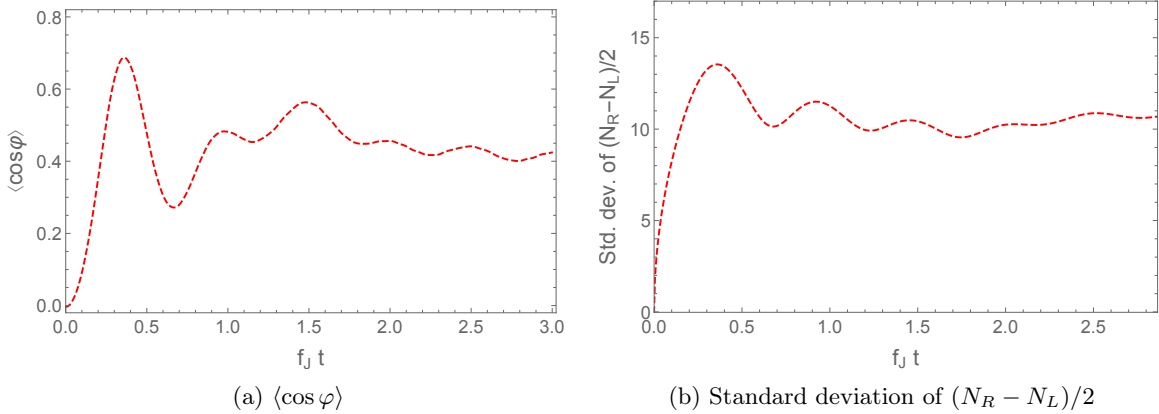


Figure 5: Time dependent expectation value of (a) $\cos \varphi$ and (b) the standard deviation of half of the particle number difference, for an experimentally accessible parameter set, calculated within TWA. We used the particle number $N = 1000$, system size $L = 25\mu m$, tunnel coupling $J/\hbar = 30\text{Hz}$, and Luttinger parameter $K = 27$. For a condensate of ^{87}Rb atoms, with atomic mass m_{Rb} , this corresponds to $c = 830\mu m/s$, and typical short distance cutoff $\xi_h \equiv \hbar/(m_{\text{Rb}}c) = 0.62\mu m$, consistent with the number of lattice sites $N_s = L/\xi_h = 28$. Time is measured in terms of the bare Josephson frequency, $f_J = 189.7\text{Hz}$.

relaxation to $\langle \cos \varphi \rangle < 1$, consistent with previous theoretical results [31]. For the case of non-zero initial asymmetry, rapid oscillations are found whose period matches the prediction of the pendulum model to high precision, while their amplitude is modulated by some lower frequency. We were able to estimate and explain the period of this beating by considering the frequency shift between the classical trajectories of the pendulum, intersected by our initial state, though the resulting modulation frequency seems to be strongly renormalized by the $k \neq 0$ modes.

We note that the Luttinger parameter K used in our simulations is slightly out of the reach of current experimental realizations. To argue that our main findings, in particular, the clear absence of fast relaxation towards a phase locked state with $\langle \cos \varphi \rangle \approx 1$ holds for the weaker interaction strengths characterizing the currently available domain of experimental parameters, we present the results of a TWA simulation for an experimentally accessible parameter set in Fig. 5. As in Sec. 5.1, the initial state was the ground state of two identical condensates, and we found that only partial coherence is built up after the recoupling, $\langle \cos \varphi \rangle \lesssim 0.5$. Unfortunately, it is difficult to use TCSA for such weak interaction strengths, i.e. larger values of the Luttinger parameter K , because the large number of relevant Fock modules results in an intractably large Hilbert space⁵. Nevertheless, having validated the TWA by a direct comparison to TCSA in the regime of strong interactions, the TWA results in Fig. 5 provide strong evidence that the experimentally observed phase locking cannot be captured by the homogeneous sine-Gordon model considered here.

It would be interesting to have measurements directly in the range of parameters accessible by our simulations, which could pin down the time scale where the deviation between the sine-Gordon model and the coupled condensate system occurs. This could help identify the presently unknown mechanism for the experimentally found rapid phase-locking, and is probably related to other degrees of freedom of the experimental system. The effect of such degrees of freedom can also be studied by including them in the TWA and/or TCSA simulations, which is an interesting direction for future

⁵The seemingly counter-intuitive difficulties of TCSA in the regime of weak interactions are discussed at the end of Section 4.2 in more detail.

investigations.

Acknowledgements

The authors are grateful to E.G. Dalla Torre, J. Schmiedmayer and I. Mazets for useful discussions. M.K., I.L., G.T. and G.Z. are also grateful for the hospitality of the Erwin Schrödinger Institute for Mathematics and Physics during the thematic programme “Quantum Paths”, facilitating contacts with the Atomchip Group at TU Wien. This research was supported by the National Research Development and Innovation Office (NKFIH) under a K-2016 grant no. 119204 and an OTKA grant no. SNN118028, and also by the BME-Nanotechnology FIKP grant of EMMI (BME FIKP-NAT). G.T. and G.Z. acknowledge partial support by the Quantum Technology National Excellence Program (Project No. 2017-1.2.1-NKP-2017- 00001), while M.K. was also supported by a “Prémium” postdoctoral grant of the Hungarian Academy of Sciences.

References

- [1] T. Kinoshita, T. Wenger, and D.S. Weiss, *Nature* **440** (2006) 900–903.
- [2] S. Trotzky, Y.-A. Chen, A. Flesch, I.P. McCulloch, U. Schollwöck, J. Eisert and I. Bloch, *Nat. Phys.* **8** (2012) 325-330, arXiv:1101.2659 [cond-mat.quant-gas].
- [3] M. Gring, M. Kuhnert, T. Langen, T. Kitagawa, B. Rauer, M. Schreitl, I.E. Mazets, D.A. Smith, E. Demler and J. Schmiedmayer, *Science* **337** (2012) 1318-1322, arXiv:1112.0013.
- [4] T. Langen, S. Erne, R. Geiger, B. Rauer, T. Schweigler, M. Kuhnert, W. Rohringer, I.E. Mazets, T. Gasenzer and J. Schmiedmayer, *Science* **348** (2015) 207–211, arXiv:1411.7185 [cond-mat.quant-gas].
- [5] S. Hofferberth, I. Lesanovsky, B. Fischer, T. Schumm and J. Schmiedmayer, *Nature* **449** (2007) 324-327, arXiv:0706.2259 [cond-mat.other].
- [6] T. Langen, R. Geiger, M. Kuhnert, B. Rauer and J. Schmiedmayer, *Nat. Phys.* **9** (2013) 640-643, arXiv:1305.3708 [cond-mat.quant-gas].
- [7] F. Meinert, M.J. Mark, E. Kirilov, K. Lauber, P. Weinmann, A.J. Daley and H.-C. Nägerl, *Phys. Rev. Lett.* **111** (2013) 053003, arXiv:1304.2628 [cond-mat.quant-gas].
- [8] T. Fukuhara, P. Schauß, M. Endres, S. Hild, M. Cheneau, I. Bloch and C. Gross, *Nature* **502** (2013) 76-79, arXiv:1305.6598 [cond-mat.quant-gas].
- [9] A.M. Kaufman, M.E. Tai, A. Lukin, M. Rispoli, R. Schittko, P.M. Preiss and M. Greiner, *Science* **353** (2016) 794-800, arXiv: 1603.04409 [quant-ph].
- [10] M. Cheneau, P. Barmettler, D. Poletti, M. Endres, P. Schauss, T. Fukuhara, C. Gross, I. Bloch, C. Kollath and S. Kuhr, *Nature* **481** (2012) 484-487, arXiv:1111.0776 [cond-mat.quant-gas].
- [11] M. Rigol, V. Dunjko, V. Yurovsky and M. Olshanii, *Phys. Rev. Lett.* **98** (2007) 050405, arXiv: cond-mat/0604476.
- [12] S. Levy, E. Lahoud, I. Shomroni, and J. Steinhauer, *Nature* **449** (2007) 579-583.
- [13] R. Gati, M. Albiez, J. Foelling, B.Hemmerling and M.K. Oberthaler, *Appl. Phys.* **B82** (2006) 207-210, arXiv: cond-mat/0604348.

- [14] V. Gritsev, A. Polkovnikov and E. Demler, *Phys. Rev.* **B75** (2007) 174511, arXiv:cond-mat/0701421.
- [15] T. Schweigler, V. Kasper, S. Erne, B. Rauer, T. Langen, T. Gasenzer, J. Berges and J. Schmiedmayer, *Nature* **545** (2017) 323-326, arXiv:1505.03126 [cond-mat.quant-gas].
- [16] S.Beck, I.E. Mazets, and T. Schweigler: **A Non-Perturbative Method to compute Thermal Correlations in One-Dimensional Systems**, arXiv:1712.01190.
S. Beck, I.E. Mazets, and T. Schweigler, *Phys. Rev.* **A98** (2018) 023613, arXiv:1802.06610.
- [17] M. Pigneur, T. Berrada, M. Bonneau, T. Schumm, E. Demler and J. Schmiedmayer, *Phys. Rev. Lett.* **120** (2018) 173601, arXiv:1711.06635 [quant-ph].
- [18] W.E. Thirring, *Annals Phys.* **3** (1958) 91-112.
- [19] S. Coleman, *Phys. Rev.* **D11** (1975) 2088-2097.
- [20] S. Mandelstam, *Phys. Rev.* **D11** (1975) 3026-3030.
- [21] L.D. Faddeev and V.E. Korepin, *Phys. Rep.* **42** (1978) 1-87.
- [22] E.K. Sklyanin, L.A. Takhtadzhyan and L.D. Faddeev, *Theor. Math. Phys.* **40** (1979) 688-706.
- [23] A.B. Zamolodchikov, *Commun. Math. Phys.* **55** (1977) 183–186.
A.B. Zamolodchikov and Al.B. Zamolodchikov, *Annals Phys.* **120** (1979) 253–291.
- [24] S. Lukyanov and A.B. Zamolodchikov, *Nucl. Phys.* **B493** (1997) 571–587.
- [25] F.A. Smirnov, **Form Factors in Completely Integrable Models of Quantum Field Theory** (Advanced Series in Mathematical Physics). World Scientific Pub Co Inc, 1992.
- [26] F.H.L. Essler and R.M. Konik, **Applications of Massive Integrable Quantum Field Theories to Problems in Condensed Matter Physics**, in: *From Fields to Strings: Circumnavigating Theoretical Physics*, pp. 684–830. World Scientific, 2005.
- [27] F. Buccheri and G. Takács, *JHEP* **1403** (2014) 026, arXiv:1312.2623 [hep-th].
- [28] Á. Hegedűs, *JHEP* **1803** (2018) 047, arXiv:1710.09583 [hep-th].
- [29] K. Damle and S. Sachdev, *Phys. Rev. Lett.* **95** (2005) 187201, arXiv: cond-mat/0507380 [cond-mat.str-el].
- [30] M. Kormos and G. Zaránd, *Phys. Rev.* **E 93** (2016) 062101, arXiv:1507.02708 [cond-mat.stat-mech].
C.P. Moca, M. Kormos, and G. Zaránd, *Phys. Rev. Lett.* **119** (2017) 100603, arXiv:1609.00974 [cond-mat.stat-mech].
- [31] E.G. Dalla Torre, E. Demler and A. Polkovnikov, *Phys. Rev. Lett.* **110** (2013) 090404, arXiv:1211.5145 [cond-mat.quant-gas].
- [32] A. Polkovnikov, *Phys. Rev.* **A68** (2003) 053604, arXiv:cond-mat/0303628 [cond-mat.stat-mech].
- [33] A. Polkovnikov, *Annals of Phys.* **325** (2010) 1790, arXiv:cond-mat/0905.3384 [cond-mat.stat-mech].

- [34] V.P. Yurov and A.B. Zamolodchikov, *Int. J. Mod. Phys.* **A5** (1990) 3221-3246.
- [35] T. Rakovszky, M. Mestyán, M. Collura, M. Kormos, and G. Takács, *Nucl. Phys.* **B911** (2016) 805–845, arXiv:1607.01068 [cond-mat.stat-mech].
K. Hódsági, M. Kormos, and G. Takács, Quench dynamics of the Ising field theory in a magnetic field, arXiv:1803.01158.
- [36] D.X. Horváth and G. Takács, *Phys. Lett.* **B 771** (2017) 539–545, arXiv:1704.00594 [cond-mat.stat-mech].
- [37] I. Kukuljan, S. Sotiriadis and G. Takács, *Phys. Rev. Lett.* **121** (2018) 110402, arXiv:1802.08696 [cond-mat.stat-mech].
- [38] M. A. Cazalilla, *J. Phys. B: AMOP* **37** (2004) S1-S47.
- [39] V. Gritsev, A. Polkovnikov, and E. Demler, *Phys. Rev. B* **75** (2007) 174511.
- [40] I. Bloch, J. Dalibard and W. Zwerger, *Rev. Mod. Phys.* **80** (2008) 885.
- [41] M. Olshanii, *Phys. Rev. Lett.* **81** (1998) 938-941, arXiv:cond-mat/9804130.
- [42] F. D. M. Haldane, *Phys. Rev. Lett.* **47** (1981) 1840.
- [43] P. Grišins and I. Mazets, *Phys. Rev.* **A87** (2013) 013629, arXiv:1206.3430 [cond-mat.quant-gas].
- [44] M. Kuhnert, R. Geiger, T. Langen, M. Gring, B. Rauer, T. Kitagawa, E. Demler, D. Adu Smith, and J. Schmiedmayer, *Phys. Rev. Lett.* **110** (2012) 090405, arXiv:1211.5323 [cond-mat.quant-gas].
- [45] A.A. Belavin, A.M. Polyakov and A.B. Zamolodchikov, *Nucl. Phys.* **B241** (1984) 333-380.
- [46] A.B. Zamolodchikov, *Int. J. Mod. Phys.* **A 10** (1995) 1125-1150.
- [47] G. Feverati, F. Ravanini and G. Takács, *Phys. Lett.* **B 430**, 264-273 (1998), arXiv:hep-th/9803104.
- [48] L. Foini and T. Giamarchi, *Phys. Rev.* **A91** (2015) 023627, arXiv:1412.6377 [cond-mat.quant-gas].
- [49] L. Foini and T. Giamarchi, *Eur. Phys. J. Special Topics* **226** (2017) 2763-2774, arXiv:1612.01858 [cond-mat.quant-gas].
- [50] G. Feverati, K. Graham, P.A. Pearce, G.Z. Tóth, and G. Watts: A renormalization group for TCSA, arXiv: hep-th/0612203.
- [51] R.M. Konik and Y. Adamov, *Phys. Rev. Lett.* **98** (2007) 147205, arXiv:cond-mat/0701605 [cond-mat.str-el].
- [52] P. Giokas and G. Watts: The renormalization group for the truncated conformal space approach on the cylinder, arXiv:1106.2448 [hep-th].
- [53] M. Hogervorst, S. Rychkov and B.C. van Rees, *Phys. Rev.* **D91** (2015) 025005, arXiv:1409.1581 [hep-th].
- [54] M. Lencsés and G. Takács, *JHEP* **1509** (2015) 146, arXiv:1506.06477 [hep-th].
- [55] I.M. Szécsényi, G. Takács and G.M.T. Watts, *JHEP* **1308** (2013) 094, arXiv:1304.3275 [hep-th].

A Mapping the coupled condensates to the sine-Gordon model

In this Appendix we provide a few more technical details on the mapping of the coupled Lieb-Liniger model given in Eqs. (3,4) to the sine-Gordon Hamiltonian (7).

For weak interactions, by standard bosonic commutation relations, the phases and the density fluctuations of each condensate form conjugate variables, $[\delta\rho_j(x), \varphi_j(y)] = -i\delta(x-y)$. Expansion of the Lieb-Liniger Hamiltonian then yields

$$H_j^s = \int dx \left\{ \frac{g}{2} \delta\rho_j^2(x) + \frac{\hbar^2 \rho_0}{2m} [\partial_x \varphi_j(x)]^2 \right\}, \quad (60)$$

which is the Luttinger Hamiltonian used in Refs. [3, 15, 43, 44].

The Luttinger Hamiltonian provides a correct description of the long wavelength behavior even for strong interactions. Identifying now $\delta\rho_j(x)$ as $\Pi_j(x)$, we have

$$H_j^s = \frac{\hbar c}{2} \int dx \left\{ \frac{\pi}{K_s} \Pi_j^2(x) + \frac{K_s}{\pi} [\partial_x \varphi_j(x)]^2 \right\}, \quad (61)$$

where $[\varphi_j(x), \Pi_k(x')] = i\delta_{jk}\delta(x-x')$. The speed of sound c , and the Luttinger parameter K_s of a single condensate can be computed from the exact Bethe Ansatz solution of the Lieb-Liniger model (3). For small and large couplings they are given by the asymptotic formulae

$$\begin{aligned} K_s &\approx \frac{\pi}{\sqrt{\gamma}} \left(1 - \frac{\sqrt{\gamma}}{2\pi}\right)^{-1/2} \approx \hbar\pi \sqrt{\frac{\rho_0}{mg}}, & c &\approx \sqrt{\frac{\rho_0 g}{m}} & \text{for } \gamma \lesssim 10, \\ K_s &\approx (1 + 4/\gamma), & c &\approx \hbar\pi\rho_0/m & \text{for } \gamma \gg 1. \end{aligned} \quad (62)$$

Thus for $\gamma \ll 1$ Eq. (61) reduces to (60). Due to Galilean invariance, $cK_s = \hbar\rho_0\pi/m$ holds for all γ .

Density fluctuations are suppressed at wavelengths smaller than the healing length ξ_h , which also serves as a short distance cutoff. For small γ it is much longer than the particle-particle distance,

$$\xi_h = 1/(\rho_0\sqrt{\gamma}) = \hbar/\sqrt{mg\rho_0} \approx \hbar/mc, \quad (63)$$

while at strong coupling $\xi_h \approx 1/\rho_0$ [14].

The coupling between the condensates is captured by the Josephson tunneling term, which is $2J\rho_0 \cos(\varphi_1 - \varphi_2)$ for small interactions, but it can be renormalized at strong interactions [14]. The total Hamiltonian can therefore be rewritten as

$$H = H_1^s + H_2^s - 2J\rho_0 \int dx \cos(\varphi_1 - \varphi_2). \quad (64)$$

Focusing on the evolution of the relative phase $\varphi_1 - \varphi_2$, we introduce the fields

$$\begin{aligned} \varphi_r &= \varphi_1 - \varphi_2, & \varphi_t &= \frac{\varphi_1 + \varphi_2}{2} \\ \Pi_r &= \frac{\Pi_1 - \Pi_2}{2}, & \Pi_t &= \Pi_1 + \Pi_2 \end{aligned} \quad (65)$$

which satisfy the canonical commutation relations. In our approximation, relative and total phase degrees of freedom decouple with the relative phase field having the Hamiltonian (7) with the Luttinger parameter

$$K = K_r = K_s/2, \quad (66)$$

B Relating $\cos \varphi$ and $:\cos \varphi:$

As a starting point recall the lattice Hamiltonian (10):

$$H_{Lat} = \frac{\hbar c}{2} \sum_{j=1}^{N_s} \left\{ \frac{\pi}{Ka} n_j^2 + \frac{K}{\pi a} (\varphi_j - \varphi_{j-1})^2 \right\} - 2J\rho_0 a \sum_{j=1}^{N_s} \cos \varphi_j, \quad (67)$$

where a is the lattice spacing, $[\varphi_j, n_k] = i\delta_{jk}$ with $\dot{\varphi}_i = \frac{c\pi}{Ka} n_i$, $N_s = L/a$ is the number of sites, and periodic boundary conditions are assumed. Our goal is to express H_{Lat} with the normal-ordered cosine as follows

$$H_{Lat} = \frac{\hbar c}{2} \sum_{j=1}^{N_s} \left\{ \frac{\pi}{Ka} n_j^2 + \frac{K}{\pi a} (\varphi_j - \varphi_{j-1})^2 \right\} - 2J\rho_0 a \mathcal{N} \sum_{j=1}^{N_s} : \cos \varphi_j :. \quad (68)$$

Consider the mode expansion of the fields using the Fourier representation

$$\varphi_i = \tilde{\varphi}_0 + \frac{1}{\sqrt{N_s}} \sum_{k \in \frac{2\pi}{L}\mathbb{Z}, k \neq 0} e^{ikx_j} \tilde{\varphi}_k \quad (69)$$

with $x_j = ja$, as follows

$$\begin{aligned} \varphi_j &= \frac{1}{\sqrt{N_s}} \sum_{k \neq 0} A_k \left(e^{ikx_j - i\omega_k t} b_k + e^{-ikx_j + i\omega_k t} b_k^\dagger \right) + \varphi_0 + \frac{\pi_0 t}{N_s} \frac{c\pi}{Ka} \\ n_j &= \frac{1}{\sqrt{N_s}} \sum_{k \neq 0} (-i) \frac{Ka}{c\pi} \omega_k A_k \left(e^{ikx_j - i\omega_k t} b_k - e^{-ikx_j + i\omega_k t} b_k^\dagger \right) + \frac{\pi_0}{N_s}, \end{aligned} \quad (70)$$

The zero modes $\tilde{\varphi}_0 = \frac{1}{N_s} \sum_j \varphi_j$ and $\tilde{\pi}_0 = \sum_j n_j$ satisfy

$$[\tilde{\varphi}_0, \tilde{\pi}_0] = [\varphi_0, \pi_0] = i, \quad (71)$$

while choosing

$$A_k = \sqrt{\frac{c\pi}{2Ka\omega_k}} \quad (72)$$

ensures

$$[b_k, b_{k'}^\dagger] = \delta_{k,k'}. \quad (73)$$

The lattice dispersion relation stated in Eq. (11) in the main text,

$$\varepsilon_k \equiv \hbar\omega_k = \frac{2\hbar c}{a} \left| \sin \frac{ka}{2} \right|, \quad (74)$$

easily follows from the $J = 0$ equation of motion

$$\ddot{\varphi}_j = \frac{c^2}{a^2} (\varphi_{j+1} + \varphi_{j-1} - 2\varphi_j). \quad (75)$$

To relate $\cos \varphi$ with $:\cos \varphi:$, first consider the exponential

$$e^{i\varphi_j} = \prod_{k \neq 0} \exp \left(\frac{i}{\sqrt{N_s}} A_k \left(e^{ikx_j - i\omega_k t} b_k + e^{-ikx_j + i\omega_k t} b_k^\dagger \right) \right) \times \exp \left(i\varphi_0 + i \frac{\pi_0 t}{N_s} \frac{c\pi}{Ka} \right). \quad (76)$$

This can be reordered using the Baker-Campbell-Hausdorff formula,

$$e^X e^Y = e^{X+Y} e^{\frac{1}{2}c} \quad (77)$$

valid when $[X, Y] = c$ is a c -number. This results in the relation

$$\begin{aligned} : e^{i\varphi_j} : &= \mathcal{N} e^{i\varphi_j} \\ \text{with } \mathcal{N} &= \prod_{k \neq 0} \exp\left(\frac{c\pi}{2N_s a 2K \omega_k}\right) \exp\left(i \frac{tc\pi}{2N_s K a}\right). \end{aligned} \quad (78)$$

Omitting a complex phase originating from the zero mode, we arrive at

$$\cos \varphi_i = \mathcal{N} : \cos \varphi_i : \quad (79)$$

with the renormalisation factor written as

$$\begin{aligned} \mathcal{N} &= \prod_{k \neq 0} \exp\left(-\frac{\pi}{8N_s K |\sin \frac{ka}{2}|}\right) = \prod_{n=-N_s/2+1(\neq 0)}^{N_s/2} \exp\left(-\frac{\pi}{8N_s K |\sin \frac{\pi n}{N_s}|}\right) \\ &= \exp\left(-\frac{\pi \Delta}{N_s}\right) \prod_{n=1}^{N_s/2-1} \exp\left(-\frac{2\pi \Delta}{N_s \sin \frac{\pi n}{N_s}}\right), \end{aligned} \quad (80)$$

where

$$\Delta = \frac{\beta^2}{8\pi}. \quad (81)$$

C Cut-off dependence and extrapolation in TCSA

TCSA inevitably involves an energy cut-off e_{cut} to truncate the Hilbert space to a finite dimensional one. Therefore all quantities computed from TCSA possess a cut-off dependence which can be addressed using renormalisation group methods [50, 51, 52, 53, 54]. Here we avoid the technical details and simply present the relevant results for expectation values of local operators together with a heuristic justification borrowed from [55].

Let us denote the vacuum expectation value of a local operator in the sine-Gordon TCSA with a cut-off parametrized as

$$n = \frac{e_{\text{cut}}}{2} \quad (82)$$

as $\langle \mathcal{O} \rangle^{(n)}$. It was shown in [55] that the leading cut-off dependence can be written as

$$\langle \mathcal{O} \rangle^{(n)} = \langle \mathcal{O} \rangle^{(\infty)} + \sum_A K_A n^{2\alpha_A - 2} \left(1 + O\left(\frac{1}{n}\right)\right), \quad (83)$$

where $\langle \mathcal{O} \rangle^{(\infty)}$ is the expectation value with the cut-off removed. Using this relation, data points obtained for a sequence of sufficiently high n can be extrapolated numerically to obtain a precise estimate for the expectation value $\langle \mathcal{O} \rangle^{(\infty)}$. The exponents α_A in (83) can be analytically determined via the operator product expansion (OPE) of the perturbing field V (i.e. the cosine potential for the sine-Gordon theory) and the operator \mathcal{O} . According to the OPE, the short distance singularity of operator products (inserted into correlation functions) is given by

$$\mathcal{O}(z, \bar{z})V(w, \bar{w}) \sim \sum_A \frac{C_{\mathcal{O}V}^A A(w, \bar{w})}{(z-w)^{(h_O+h_V-h_A)} (\bar{z}-\bar{w})^{(\bar{h}_O+\bar{h}_V-\bar{h}_A)}}, \quad (84)$$

where A runs over a complete set of local operators, and h and \bar{h} are the right and left conformal weights of the operators. For scalar operators satisfying $h = \bar{h}$, α_A is given by

$$\alpha_A = h_O + h_V - h_A. \quad (85)$$

For a heuristic understanding of the expression (83) note that the running coupling characterizing a relevant operator becomes small at high energy (i.e. short distance) scales. Therefore as the dependence of expectation values on large values of the cut-off n are concerned, the corrections to the exact expectation value $\langle T\mathcal{O} \exp(-\lambda \int d^2z V) \rangle$ can be replaced by ones computed from the first order perturbative expression $-\lambda \langle T\mathcal{O} \int d^2z V \rangle$. The OPE yields

$$\mathcal{O} \int d^2z V \sim \sum_A C_{AA}, \quad (86)$$

where the dimensions of the coefficients C_A are $[\text{energy}]^{-2+2\alpha_A}$. For a large cut-off n , the associated energy scale $\frac{4\pi}{L}n$ is much larger than any other scale in the theory and is therefore the only relevant energy scale. Therefore a simple scaling argument predicts that the cut-off dependence of $\langle \mathcal{O} \rangle^{(n)}$ must be of the form $n^{2\alpha_A-2}$. In practical application, it is usually enough to keep the largest one among the exponents α_A predicted by the OPE.

For the particular case of sine-Gordon model, α_A can be calculated by using the conformal weight of the vertex operators V_a ,

$$h_a = \bar{h}_a = a^2\Delta, \quad (87)$$

whereas the conformal weight of the derivative operator $\partial\phi\bar{\partial}\phi$ is $h = 1$. The fusion rules for the vertex operators V_a and V_b encoding the possible operator families entering their OPE reads

$$[V_a] \times [V_b] = [V_{a+b}], \quad (88)$$

where $[V_a]$ signifies the appearance of the vertex operator (primary) and its descendants, which are obtained by multiplying the exponential with a polynomial expression of the derivatives of ϕ . The perturbing cosine of the sine-Gordon model is given by the combination $V_1 + V_{-1}$. For the observable $\mathcal{O} =: \cos\beta\phi := (V_1 + V_{-1})/2$, the fusion rules imply that the families of the \mathcal{I} (i.e. V_0) and $V_{\pm 2}$ enter the relevant OPE, yielding the exponents $n^{-2+4\Delta}$, $n^{-4+2\Delta}$ and $n^{-2-4\Delta}$ for $A = \mathcal{I}$, $\partial\phi\bar{\partial}\phi$ and $:\cos 2\beta\phi:$ (here $\partial\phi\bar{\partial}\phi$ appears as the descendant field of \mathcal{I}). For the observable $:\sin\beta\phi:$ one obtains a similar result.

The particle number difference $N_R - N_L$ is given as a spatial integral of the field momentum $\partial_t\phi = \partial\phi + \bar{\partial}\phi$, which is a combination of operators of weights $(1, 0)$ and $(0, 1)$ which have non-zero spins. However, a simple application of the heuristic scaling argument using the following OPEs (resulting from Wick's theorem for the free massless boson ϕ)

$$\begin{aligned} \partial\phi(z, \bar{z})V_a(w, \bar{w}) &\propto \frac{iaV_a(w, \bar{w})}{z-w} + \text{regular terms}, \\ \bar{\partial}\phi(z, \bar{z})V_a(w, \bar{w}) &\propto \frac{iaV_a(w, \bar{w})}{\bar{z}-\bar{w}} + \text{regular terms}, \end{aligned} \quad (89)$$

allows one to determine the cut-off exponent. In this case we have a separate exponent for the singular behavior of left/right movers, e.g. for $\partial\phi$ we have

$$\alpha = h_{\partial\phi} + h_{V_a} - h_{V_a} = 1 \quad \bar{\alpha} = \bar{h}_{\partial\phi} + \bar{h}_{V_a} - \bar{h}_{V_a} = 0 \quad (90)$$

leads to the naive value $-2 + \alpha + \bar{\alpha} = -1$ for the extrapolation exponent (similarly for $\bar{\partial}\phi$ with the values of α and $\bar{\alpha}$ interchanged). However, note that the actual perturbing operator is $V_{+1} + V_{-1}$, and so the leading term cancels for the combination $\partial_t\phi = \partial\phi + \bar{\partial}\phi$. The next-to-leading coefficient results from considering level 1 descendent contributions, which leads to the cut-off exponent -2 . For the variance of $N_R - N_L$, it is necessary to consider the operator product with $\partial_t\phi(z_1, \bar{z}_1)\partial_t\phi(z_2, \bar{z}_2)$; a straightforward application of the Wick theorem to compute the free boson OPE then results in a cut-off exponent -2 .

We finish this section with two important comments. Firstly, although the above discussion of the cut-off dependence of one point functions assumed the case of vacuum expectation values, the leading order cut-off dependence is determined by the universal OPE exponents and is therefore the same for expectation values in excited states. The only difference is that for the validity of the leading order cut-off extrapolation the cut-off must also be large enough compared to the energy of the excited state under consideration.

Secondly, further improvements can be made by adding explicit counter terms to the TCSA Hamiltonian and also to the operator [36, 54], whose coefficients are determined by renormalisation group equations similar to (83). However, in the context of the present work the using the leading order expressions for such counter-terms did not result in any notable improvement compared to the simple extrapolation procedure sketched above, therefore they were omitted to reduce the computational costs.

D Expansion of Keldysh path integral

In this appendix we outline the expansion of the Keldysh path integral in terms of quantum fields, following Refs. [32, 33]. In App. D.1 we derive the TWA result (34) as the leading order of this expansion, while in App. D.2 we determine the next quantum correction to the TWA.

D.1 Derivation of TWA

In this section we first derive (34) for a general time-dependent Hamiltonian $\hat{H}(t)$ expressed in terms of the canonical conjugate phase and particle number operators $\{\hat{\varphi}_i, \hat{n}_i\}$, and then we specialize the results to Hamiltonian (10). Here we denote every operator by a hat, i.e. such as \hat{X} to distinguish them from the ordinary variables X entering the path integral.

For an initial density matrix $\hat{\rho}_0$, the out-of-equilibrium expectation value of the operator of interest, $\hat{\mathcal{O}}$, can be expressed as

$$\langle\hat{\mathcal{O}}\rangle(t) = \text{Tr} \left(\hat{\rho}_0 \mathcal{T} e^{-i/\hbar \int_{\mathcal{C}_-} dt' \hat{H}(t')} \hat{\mathcal{O}} e^{-i/\hbar \int_{\mathcal{C}_+} dt' \hat{H}(t')} \right). \quad (91)$$

Here the operator \mathcal{T} stands for the ordering along the Keldysh contour consisting of forward and backward branches \mathcal{C}_+ and \mathcal{C}_- , with turning point t , depicted in Fig. 6.

To evaluate the expectation value (91), the time is discretized in steps $\Delta t = t/M$, and the first completeness relation of (30) is inserted at every site j after each time step on both branches (see Fig. 6). The eigenvalue of the phase operator $\hat{\varphi}_j$ at time $m\Delta t$ is denoted by $\varphi_{j,m}^\pm$ on the contour $\mathcal{C}_+/\mathcal{C}_-$. Similarly to the notations of Sec. 4.1, we introduce a more compact vector notation

$$\underline{\varphi}_m^\pm = \{\varphi_{j,m}^\pm\}$$

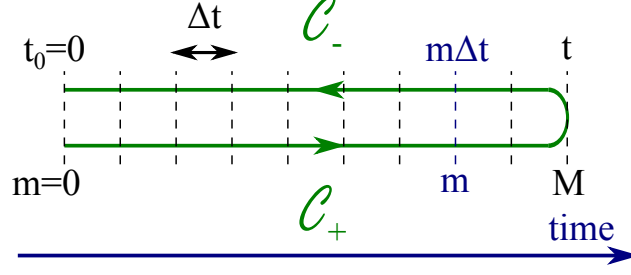


Figure 6: Keldysh contour. The contour of the path integral in Eq. (91), running from $t_0 = 0$ to t , consisting of forward (\mathcal{C}_+) and backward (\mathcal{C}_-) branches. All operators are ordered along the Keldysh contour. The path integral can be evaluated by introducing a discrete time step $\Delta t = t/M$, and inserting the completeness relation (30) at each time step according to Eq. (92).

for the full set of eigenvalues at a given time step m , with analogous notations for the eigenvalues of the operators \hat{n}_j . In the following $\hat{H}(m\Delta t)$ is abbreviated by \hat{H}_m , also allowing for an explicit time-dependence of the Hamiltonian.

With these notations, the expectation value (91) can be rewritten as

$$\begin{aligned} \langle \hat{\mathcal{O}} \rangle(t) &= \int \mathcal{D}\varphi \langle \varphi_0^+ | \hat{\rho}_0 | \varphi_0^- \rangle \prod_{m=0}^{M-1} \langle \varphi_m^- | e^{i\Delta t \hat{H}_{m+1}/\hbar} | \varphi_{m+1}^- \rangle \langle \varphi_M^- | \hat{\mathcal{O}} | \varphi_M^+ \rangle \prod_{m=1}^M \langle \varphi_m^+ | e^{-i\Delta t \hat{H}_{m-1}/\hbar} | \varphi_{m-1}^+ \rangle = \\ &= \int \mathcal{D}\varphi \mathcal{D}n \langle \varphi_0^+ | \hat{\rho}_0 | \varphi_0^- \rangle \prod_{m=0}^{M-1} e^{i\varphi_m^- n_m^-} \langle n_m^- | e^{i\Delta t \hat{H}_{m+1}/\hbar} | \varphi_{m+1}^- \rangle \langle \varphi_M^- | \hat{\mathcal{O}} | \varphi_M^+ \rangle \prod_{m=1}^M e^{i\varphi_m^+ n_m^+} \langle n_m^+ | e^{-i\Delta t \hat{H}_{m-1}/\hbar} | \varphi_{m-1}^+ \rangle, \end{aligned} \quad (92)$$

with

$$\mathcal{D}\varphi = \frac{1}{(2\pi)^{2N_s(M+1)}} \prod_{m=0}^M d\varphi_m^+ d\varphi_m^-, \quad \mathcal{D}n = \prod_{m=1}^M dn_m^+ dn_m^-. \quad (93)$$

The second equality in (92) was obtained by inserting the second completeness relation of (30) at each time step, and applying (29). Assuming that $\hat{H}(t)$ is written in a normal ordered form, the matrix elements of the propagator are given by

$$\langle n | e^{-i\Delta t \hat{H}_m/\hbar} | \varphi \rangle = e^{-i\varphi n} e^{-i\Delta t H_m(n, \varphi)/\hbar} + O(\Delta t^2), \quad (94)$$

where $H_m(n, \varphi)$ is obtained by substituting every operator $\hat{\varphi}_j$ or \hat{n}_j in \hat{H}_m by the corresponding eigenvalue φ_j and n_j , respectively. This relation allows to express the expectation value (92) as

$$\begin{aligned} \langle \hat{\mathcal{O}} \rangle(t) &= \int \mathcal{D}\varphi \mathcal{D}n \langle \varphi_0^+ | \hat{\rho}_0 | \varphi_0^- \rangle \langle \varphi_M^- | \hat{\mathcal{O}} | \varphi_M^+ \rangle e^{i \sum_{m=0}^{M-1} n_m^- (\varphi_m^- - \varphi_{m+1}^-) + i \sum_{m=1}^M n_m^+ (\varphi_m^+ - \varphi_{m-1}^+)} \\ &= e^{i\Delta t/\hbar \sum_{m=1}^M \{ H_m(n_{m-1}^-, \varphi_m^-) - H_{m-1}(n_m^+, \varphi_{m-1}^+) \}}. \end{aligned} \quad (95)$$

We now introduce the classical and quantum components of the fields φ and n by performing the Keldysh rotation

$$\begin{aligned} \varphi_m^{cl} &= \frac{\varphi_m^+ + \varphi_m^-}{2}, & \varphi_m^q &= \varphi_m^+ - \varphi_m^-, \\ n_m^{cl} &= \frac{n_m^+ + n_{m-1}^-}{2}, & n_m^q &= n_m^+ - n_{m-1}^-. \end{aligned} \quad (96)$$

Note that the particle number on the backward path, \underline{n}^- , is shifted by one time slice in (96) compared to the other fields, ensuring that the Keldysh action vanishes for purely classical fields (i.e. when $\underline{\varphi}^q = \underline{n}^q = 0$). The origin of this index shift can be understood by noting that the canonical conjugate variables φ and n play a role analogous to the position x and momentum p/\hbar in ordinary point-particle dynamics. In the path integral formalism the coordinates are located on the time slices, while the momenta are assigned to the links between them. The rotation (96) is introduced in such a way that the quantum fields vanish, if the backward path is the time reversal of the forward path. As illustrated in Fig. 7, this prescription requires to shift the momenta – or particle numbers – of the backward path by one time slice, in accordance with (96).

Using the new variables introduced in Eq. (96), the expectation value $\langle \hat{\mathcal{O}} \rangle(t)$ can be rewritten as

$$\begin{aligned} \langle \hat{\mathcal{O}} \rangle(t) = & \int \mathcal{D}\varphi \mathcal{D}n \langle \underline{\varphi}_0^{cl} + \underline{\varphi}_0^q/2 | \hat{\rho}_0 | \underline{\varphi}_0^{cl} - \underline{\varphi}_0^q/2 \rangle \langle \underline{\varphi}_M^{cl} - \underline{\varphi}_M^q/2 | \hat{\mathcal{O}} | \underline{\varphi}_M^{cl} + \underline{\varphi}_M^q/2 \rangle \times \\ & e^{i\underline{\varphi}_M^q \underline{n}_M^{cl} - i\underline{\varphi}_0^q \underline{n}_1^{cl}} e^{i \sum_{m=1}^M \underline{n}_m^q (\underline{\varphi}_m^{cl} - \underline{\varphi}_{m-1}^{cl}) - i \sum_{m=1}^{M-1} \underline{\varphi}_m^q (\underline{n}_{m+1}^{cl} - \underline{n}_m^{cl})} \times \\ & e^{i\Delta t/\hbar \sum_{m=1}^M \left\{ H_m(\underline{n}_m^{cl} - \underline{n}_m^q/2, \underline{\varphi}_m^{cl} - \underline{\varphi}_m^q/2) - H_{m-1}(\underline{n}_{m-1}^{cl} + \underline{n}_m^q/2, \underline{\varphi}_{m-1}^{cl} + \underline{\varphi}_{m-1}^q/2) \right\}}. \end{aligned} \quad (97)$$

In accordance with the remark above, the exponent in the integrand vanishes for purely classical fields, $\underline{\varphi}^q = \underline{n}^q = 0$ when neglecting terms of order Δt^2 that disappear anyway in the limit $\Delta t \rightarrow 0$. This is a generic property ensuring the causality structure of the Keldysh action.

Dropping boundary terms which tend to zero for $\Delta t \rightarrow 0$, the integral over $\underline{\varphi}_0^q$ can be performed, yielding

$$\int d\underline{\varphi}_0^q \langle \underline{\varphi}_0^{cl} + \underline{\varphi}_0^q/2 | \hat{\rho}_0 | \underline{\varphi}_0^{cl} - \underline{\varphi}_0^q/2 \rangle e^{-i\underline{\varphi}_0^q \underline{n}_1^{cl}} = (2\pi)^{2N_s} W(\underline{\varphi}_0^{cl}, \underline{n}_1^{cl}). \quad (98)$$

Similarly, integrating over $\underline{\varphi}_M^q$ results in

$$\int d\underline{\varphi}_M^q \langle \underline{\varphi}_M^{cl} - \underline{\varphi}_M^q/2 | \hat{\mathcal{O}} | \underline{\varphi}_M^{cl} + \underline{\varphi}_M^q/2 \rangle e^{i\underline{\varphi}_M^q \underline{n}_M^{cl}} = (2\pi)^{N_s} O_W(\underline{\varphi}_M^{cl}, \underline{n}_M^{cl}). \quad (99)$$

The truncated Wigner approximation (TWA) is obtained by substituting these expressions into Eq. (97), and expanding the exponent in the path integral up to first order in quantum fields,

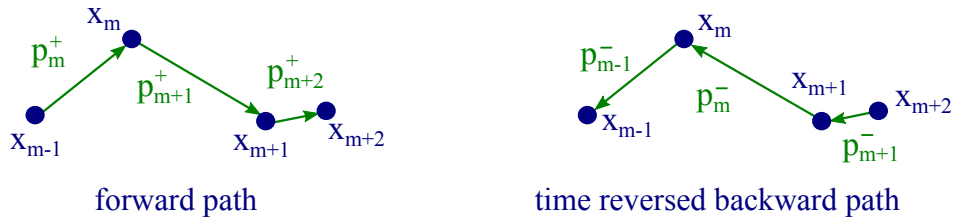


Figure 7: The drawing shows time reversed pairs of forward and backward paths, utilizing the analogy $\varphi \leftrightarrow x$ and $n \leftrightarrow p/\hbar$. Such pairs only contribute to the classical fields in Eq. (96), while they yield vanishing quantum fields.

yielding

$$\begin{aligned}
\langle \hat{\mathcal{O}} \rangle_{TW}(t) &= \int \mathcal{D}\varphi \mathcal{D}\underline{n} W(\underline{\varphi}_0^{cl}, \underline{n}_1^{cl}) O_W(\underline{\varphi}_M^{cl}, \underline{n}_M^{cl}) e^{-i \sum_{m=1}^{M-1} \underline{\varphi}_m^q \{ \underline{n}_{m+1}^{cl} - \underline{n}_m^{cl} + \Delta t \nabla_{\varphi} H_m(\underline{n}_m^{cl}, \underline{\varphi}_m^{cl}) / \hbar \}} \times \\
&\quad e^{i \sum_{m=1}^M \underline{n}_m^q \{ \underline{\varphi}_m^{cl} - \underline{\varphi}_{m-1}^{cl} - \Delta t \nabla_n H_{m-1}(\underline{n}_m^{cl}, \underline{\varphi}_{m-1}^{cl}) / \hbar \}} \\
&= \int \mathcal{D}\varphi^{cl} \mathcal{D}\underline{n}^{cl} W(\underline{\varphi}_0^{cl}, \underline{n}_1^{cl}) O_W(\underline{\varphi}_M^{cl}, \underline{n}_M^{cl}) \prod_{m=1}^{M-1} \delta \left(\underline{n}_{m+1}^{cl} - \underline{n}_m^{cl} + \Delta t \nabla_{\varphi} H_m(\underline{n}_m^{cl}, \underline{\varphi}_m^{cl}) / \hbar \right) \times \\
&\quad \prod_{m=1}^M \delta \left(\underline{\varphi}_m^{cl} - \underline{\varphi}_{m-1}^{cl} - \Delta t \nabla_n H_{m-1}(\underline{n}_m^{cl}, \underline{\varphi}_{m-1}^{cl}) / \hbar \right). \tag{100}
\end{aligned}$$

Here $\nabla_{\varphi} H$ and $\nabla_n H$ denote the gradient of the Hamiltonian:

$$(\nabla_{\varphi} H)_j = \frac{\partial H}{\partial \varphi_j} \quad \text{and} \quad (\nabla_n H)_j = \frac{\partial H}{\partial n_j}, \tag{101}$$

and second line of Eq. (34) was obtained by performing the integrals over the quantum fields using

$$\int d\underline{\varphi}_q e^{-i\underline{\varphi}_q \underline{x}} = \int d\underline{n}_q e^{i\underline{n}_q \underline{x}} = (2\pi)^{N_s} \delta(\underline{x}). \tag{102}$$

Rewriting Eq. (100) in a more compact form gives precisely Eq. (34), with the trajectories $\underline{\varphi}(t')$ and $\underline{n}(t')$ following the classical equations of motion,

$$\begin{aligned}
\partial_t \underline{n} &= -\nabla_{\varphi} H(\underline{n}, \underline{\varphi}, t) / \hbar, \\
\partial_t \underline{\varphi} &= \nabla_n H(\underline{n}, \underline{\varphi}, t) / \hbar, \tag{103}
\end{aligned}$$

solved for initial conditions $\{\underline{\varphi}_0, \underline{n}_0\}$. For the special case of Hamiltonian (10), these differential equations take the form stated in Eq. (35).

D.2 Quantum corrections to TWA quantities

In this Appendix we derive the next quantum correction to the truncated Wigner approximation (34), by expanding the exponent in Eq. (97) up to third order in the quantum fields. Here we restrict our attention to the specific Hamiltonian (10), which has a single such term of the form $(\varphi^q)^3$; the generalization for more complicated Hamiltonians is straightforward.

By expanding the integrand in (97) as

$$e^{-i\varphi_{j,m}^q x_1 - i(\varphi_{j,m}^q)^3 x_2} \approx e^{-i\varphi_{j,m}^q x_1} \left(1 - i \left(\varphi_{j,m}^q \right)^3 x_2 \right), \tag{104}$$

and substituting (32) and (33) into Eq. (97), the following correction term is obtained:

$$\begin{aligned}
\delta \langle \mathcal{O} \rangle_1(t) &= -i \frac{\Delta t}{24 \hbar} \int \mathcal{D}\varphi \mathcal{D}\underline{n} W(\underline{\varphi}_0^{cl}, \underline{n}_1^{cl}) O_W(\underline{\varphi}_M^{cl}, \underline{n}_M^{cl}) e^{-i \sum_{m=1}^{M-1} \underline{\varphi}_m^q \{ \underline{n}_{m+1}^{cl} - \underline{n}_m^{cl} + \Delta t \nabla_{\varphi} H(\underline{n}_m^{cl}, \underline{\varphi}_m^{cl}) / \hbar \}} \times \\
&\quad e^{i \sum_{m=1}^M \underline{n}_m^q \{ \underline{\varphi}_m^{cl} - \underline{\varphi}_{m-1}^{cl} - \Delta t \nabla_n H(\underline{n}_m^{cl}, \underline{\varphi}_{m-1}^{cl}) / \hbar \}} \sum_{m'=1}^{M-1} \sum_{j=1}^{N_s} \left(\varphi_{j,m'}^q \right)^3 \left. \frac{\partial^3 H}{\partial \varphi_j^3} \right|_{\underline{\varphi}_{m'}^{cl}}, \tag{105}
\end{aligned}$$

which can be written as

$$\begin{aligned} \delta\langle\mathcal{O}\rangle_1(t) &= -i\frac{\Delta t}{24\hbar} \int \mathcal{D}\varphi^{cl} \mathcal{D}n^{cl} W(\underline{\varphi}_0^{cl}, \underline{n}_1^{cl}) O_W(\underline{\varphi}_M^{cl}, \underline{n}_M^{cl}) \prod_{m=1}^M \delta\left(\underline{\varphi}_m^{cl} - \underline{\varphi}_{m-1}^{cl} - \Delta t \nabla_n H_{m-1}(\underline{n}_m^{cl}, \underline{\varphi}_{m-1}^{cl})/\hbar\right) \times \\ &\sum_{m'=1}^{M-1} \sum_{j=1}^{N_s} \frac{\partial^3 H}{\partial \varphi_j^3} \Bigg|_{\underline{\varphi}_{m'}^{cl}} \delta^{(3)}\left(\underline{n}_{m'+1}^{cl} - \underline{n}_{m'}^{cl} + \Delta t \nabla_\varphi H(\underline{n}_{m'}^{cl}, \underline{\varphi}_{m'}^{cl})/\hbar\right) \prod_{\substack{m=1 \\ m \neq m'}}^{M-1} \delta\left(\underline{n}_{m+1}^{cl} - \underline{n}_m^{cl} + \Delta t \nabla_\varphi H_m(\underline{n}_m^{cl}, \underline{\varphi}_m^{cl})/\hbar\right). \end{aligned} \quad (106)$$

where the integral over $\varphi_{j,m'}^q$ was performed using

$$\int dy y^3 e^{-ixy} = i^3 \frac{\partial^3}{\partial x^3} \int dy e^{-ixy} = -i 2\pi \delta^{(3)}(x). \quad (107)$$

After a partial integration over $n_{j,m'+1}^{cl}$, this correction term can be expressed as

$$\begin{aligned} \delta\langle\mathcal{O}\rangle_1(t) &= -i\frac{J\rho_0 a \Delta t}{12\hbar} \sum_{m'=1}^{M-1} \sum_{j=1}^{N_s} \int \mathcal{D}\varphi^{cl} \mathcal{D}n^{cl} \sin \varphi_{i,m'}^{cl} W(\underline{\varphi}_0^{cl}, \underline{n}_1^{cl}) \times \\ &\prod_{m=1}^{m'} \left[\delta\left(\underline{\varphi}_m^{cl} - \underline{\varphi}_{m-1}^{cl} - \Delta t \nabla_n H(\underline{n}_m^{cl}, \underline{\varphi}_{m-1}^{cl})/\hbar\right) \delta\left(\underline{n}_{m+1}^{cl} - \underline{n}_m^{cl} + \Delta t \nabla_\varphi H(\underline{n}_m^{cl}, \underline{\varphi}_m^{cl})/\hbar\right) \right] \times \\ &\frac{\partial^3}{\left(\partial n_{j,m'+1}^{cl}\right)^3} \left[\prod_{m=m'}^{M-1} \delta\left(\underline{\varphi}_{m+1}^{cl} - \underline{\varphi}_m^{cl} - \Delta t \nabla_n H(\underline{n}_{m+1}^{cl}, \underline{\varphi}_m^{cl})/\hbar\right) \times \right. \\ &\left. \prod_{m=m'+1}^{M-1} \delta\left(\underline{n}_{m+1}^{cl} - \underline{n}_m^{cl} + \Delta t \nabla_\varphi H(\underline{n}_m^{cl}, \underline{\varphi}_m^{cl})/\hbar\right) O_W(\underline{\varphi}_M^{cl}, \underline{n}_M^{cl}) \right] \end{aligned} \quad (108)$$

which can be rewritten in a more compact form as

$$\delta\langle\mathcal{O}\rangle_1(t) = -i\frac{J\rho_0 a}{12\hbar} \sum_{j=1}^{N_s} \int_0^t dt' \int d\underline{\varphi}_0^{cl} \int d\underline{n}_0^{cl} W(\underline{\varphi}_0^{cl}, \underline{n}_0^{cl}) \sin \varphi_j^{cl}(t') \frac{\partial^3}{\left(\partial n_j^{cl}(t')\right)^3} O_W(\underline{\varphi}^{cl}(t), \underline{n}^{cl}(t)), \quad (109)$$

where the trajectories $\underline{\varphi}^{cl}(t')$, $\underline{n}^{cl}(t')$ are determined by the classical equations of motion (35), with initial conditions $\{\underline{\varphi}_0^{cl}, \underline{n}_0^{cl}\}$, just as in the truncated Wigner approximation (34).

The correction term (109) can be evaluated by generating random initial conditions $\underline{\varphi}_0^{cl}$ and \underline{n}_0^{cl} from the Wigner distribution $W(\underline{\varphi}_0^{cl}, \underline{n}_0^{cl})$ of the initial state, and constructing the classical trajectories numerically using Eq. (35). The functional derivative with respect to $n_j^{cl}(t')$ appearing in Eq. (109) can be determined numerically by adding a small "kick" to the trajectory at time t' :

$$n_j^{cl}(t') \rightarrow n_j^{cl}(t'; \varepsilon) = n_j^{cl}(t') + \varepsilon, \quad (110)$$

which is then propagated to time t using the equations of motion (35). Calculating the modified trajectory $\{\underline{\varphi}^{cl}(t; \varepsilon), \underline{n}^{cl}(t; \varepsilon)\}$ for different kick sizes $\pm\varepsilon$ and $\pm 2\varepsilon$, the functional derivative can be evaluated by using the finite difference expression

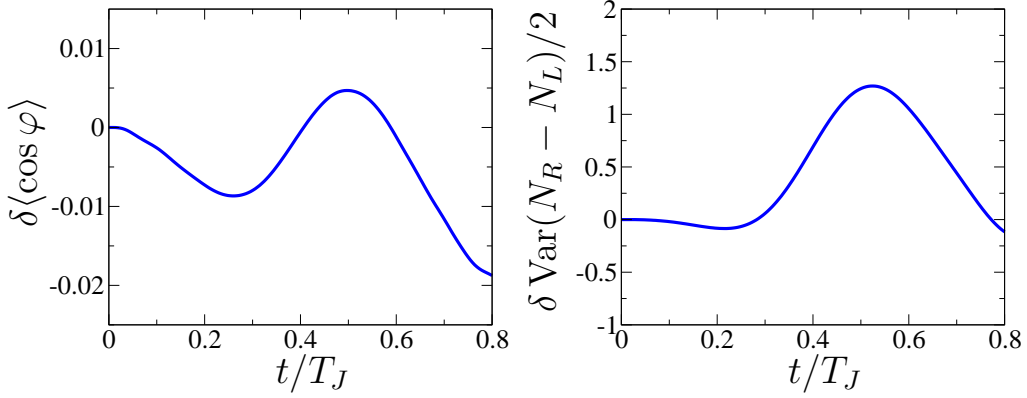


Figure 8: First quantum correction to the TWA result. The correction term, Eq. (109), for the operators $\cos \hat{\varphi}$ and $(\hat{N}_R - \hat{N}_L)^2/4$, plotted as a function of dimensionless time $f_J t$, for a quench re-coupling two independent, identical condensates prepared in their ground state. Here we use the parameters of Fig. 2: $K = 1.56$, $L = 14.86 \mu\text{m}$, $N = 400$, $c = 2800 \mu\text{m/s}$ and $J/h = 7\text{Hz}$, with the number of lattice sites $N_s = 60$. The leading order results for the time evolution of this quench were analyzed in Sec. 5.1.

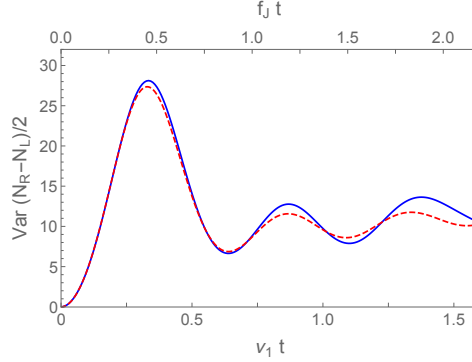


Figure 9: Time evolution of the variance of half of the particle number difference, for the initial state and parameters of Fig. 2, with continuous blue and dashed red curves corresponding to TCSA and TWA, respectively. The parameters are $K = 1.56$, $L = 14.86 \mu\text{m}$, $N = 400$, $c = 2800 \mu\text{m/s}$, $J/h = 7\text{Hz}$ and $N_s = 60$. Time is measured in terms of the bare and renormalised Josephson frequencies f_J and ν_1 in TWA and TCSA, respectively.

$$\frac{\partial^3}{(\partial n_j^{cl}(t'))^3} O_W(\underline{\varphi}^{cl}(t), \underline{n}^{cl}(t)) = \frac{1}{2\varepsilon^3} \left[O_W(\underline{\varphi}^{cl}(t; 2\varepsilon), \underline{n}^{cl}(t; 2\varepsilon)) - O_W(\underline{\varphi}^{cl}(t; -2\varepsilon), \underline{n}^{cl}(t; -2\varepsilon)) \right. \\ \left. - 2 O_W(\underline{\varphi}^{cl}(t; \varepsilon), \underline{n}^{cl}(t; \varepsilon)) + 2 O_W(\underline{\varphi}^{cl}(t; -\varepsilon), \underline{n}^{cl}(t; -\varepsilon)) \right]. \quad (111)$$

The time evolution of the quantum correction term (109) for the operators $\cos \hat{\varphi}$ and $(\hat{N}_R - \hat{N}_L)^2/4$ is illustrated in Fig. 8. Here we considered a quench already investigated in Sec. 5.1, starting with two independent identical condensates in their ground states and using the parameters

of Fig. 2. In this case the expectation value of $(\hat{N}_R - \hat{N}_L)^2/4$ coincides with the variance of the particle number difference $(\hat{N}_R - \hat{N}_L)/2$, because $\langle \hat{N}_R - \hat{N}_L \rangle = 0$ due to left-right symmetry. Since in Sec. 5.1 we plotted the standard deviation of $(N_R - N_L)/2$ instead of the variance, for better comparison we display $\text{Var}(N_R - N_L)/2$ in Fig. 9 for the parameters of Figs. 2 and 8. By comparing Fig. 8 to Figs. 2 and 9, we find that the quantum correction terms are not negligible even on quite short time scales compared to the leading contributions. Nevertheless, the good agreement between the TCSA and TWA results, demonstrated in Sec. 5.1, shows that the correction term plotted in Fig. 8 considerably overestimates the error, and the TWA yields a good approximation for the expectation values of $\cos \hat{\varphi}$ and $(\hat{N}_R - \hat{N}_L)^2/4$.